Scientific Journal of University of Benghazi

SJUOB (2025) 38 (2) Applied Sciences: Mohammed. et . al, 73 – 93
www.sjuob.uob.edu.ly

Developing and Evaluating an Explainable Deep Learning–Based User Interface for Libyan Currency Authentication.

Mohammed Masoud Mohammed[1]*, Aeman.I.G.Masbah[2], Mansaf M. Elmansori[2]

1. Department of Computer Science, Faculty of Science, Derna University, Libya.

2. Department of Computer, College of Technical Sciences - Derna, Libya.

DOI: 10.37376/sjuob.v38i2 | Received:15/09/2025 | Accepted:21/11/2025 | Publishing: 23/12/2025

ABSTRACT

The problem of counterfeit currency production and distribution is increasing, driven by technological advancements, particularly the development of advanced printing machines. The ongoing issue of counterfeit currency poses a significant threat to the national economy, necessitating the creation of an effective detection system. In light of this problem, this study proposes an intelligent system for identifying and detecting counterfeit Libyan currency. This system relies on deep learning techniques. Our proposed model is based on the EfficientNet-B4 controlled architecture, which seeks to optimize computing power and accuracy. In this study, the dataset was prepared and preprocessed using Gaussian filtering to reduce noise and normalize. The general framework developed here consists of two stages: The first stage is an intelligent filter that attempts to exclude any banknotes or images that are not Libyan currency, ensuring that only data related to Libyan banknotes is transmitted to the second stage of the model. The second stage is the core of the study, as it will determine whether Libyan currency is authentic or counterfeit. To improve the transparency of the model and enhance the understanding of its results, Grad-CAM software was used to generate heat maps that clearly show the banknote regions that contributed most to the model's decision-making. To demonstrate the system's usability, a mock-up user interface was designed to illustrate the system's analysis and provide a practical environment. The results demonstrated good classification performance, consistently exceeding 90%, demonstrating how the proposed approach can be effectively applied to these models in practical situations. The findings of this research provide a practical framework to help financial institutions mitigate counterfeiting as part of the relevant compliance objectives that will determine the security of the monetary system.

KEYWORDS: Libyan Currency, Counterfeit Detection, Image Classification, Deep Learning, Efficientnet-B4, Heatmap Visualization, Grad-CAM, User Interface.

Corresponding Author: Mohammed Masoud Mohammed, mohammed.bwshnaty@gmail.com

 ISSN: Online 2790-1637, Print 2790-1629
National Library of Libya, Legal number: 154/2018

1.INTRODUCTION

In today's continually evolving world, technology is changing at an unprecedented rate that causes an unimaginable degree of change in our lives and work. While these advancements have undoubtedly enhanced convenience, they have also created opportunities for various forms of misuse. The most notable is counterfeiting banknotes. Counterfeiting is not a new concern; it has existed for generations. However, new technologies increase the liabilities associated with counterfeiting. While measures have improved a lot in terms of increased security features in different denominations, and overall banknote security has improved, the skill of counterfeiting has also improved in a way that makes it difficult to differentiate between genuine and fake notes [1]. This problem is especially prevalent in countries that are politically and economically unstable. In these situations, without proper regulatory scrutiny, a burgeoning black market has spread counterfeit currency, which invariably threatens the financial system and undermines public confidence in the national currency. Moreover, it has economic implications, as the effects of currency forgery also present significant security and social challenges by disrupting the functioning of markets, obstructing normal operations for businesses, and increasing the workload of financial and security actors [2]. Paper money is still widely used in everyday transactions, even with the numerous solutions that have been put forth to lessen dependency on actual cash, such as smart cards, magnetic cards, and electronic payment systems. Because of this reliance on cash, counterfeiters continue to have opportunities to take advantage of the system. Therefore, we desperately need a reliable system that can differentiate between real and fake banknotes based on their visual characteristics [3-4]. When dealing with high-quality counterfeit copies, traditional verification methods such as visual inspection and ultraviolet (UV) analysis have proven ineffective. The situation requires the use of modern technology tools to provide more reliable and permanent alternatives for fraud detection. Counterfeit detectors are often available in banks, and these devices are not easily accessible to the general public. Given these limitations, the field needs a more accessible and user-friendly way to develop public confidence in currencies[5]. In that aspect, advanced technology in encompassing methods based on deep learning has demonstrated potential, most notably in image studies and with the identified subtle visual cues not easily observed by humans. The aim of this study is to devise an intelligent system that can detect and recognize authentic or counterfeit Libyan paper currency using current technology without using complicated or costly instruments. This study is accomplished by determining if any discrepancies or divergences are identified, which hints that the currency is counterfeit. Its ability to detect counterfeit bills accurately, quickly, and at low cost is of great value to banks, agencies of government, businesses, and the general public. Last, but not least, it is also an original way to keep up with technical advancements while utilizing sophisticated computational mechanisms for the benefit of the economy of Libya.

1.1.Deep Learning in Image Classification:

Deep Learning (DL) is a growing form of machine learning (ML), a form of artificial intelligence (AI), as shown in Figure 1. DL is built on multi-layer or "deep" neural networks (DNNs). This form of machine learning has become a game-changing technology in computer vision, notably with image classification [6].

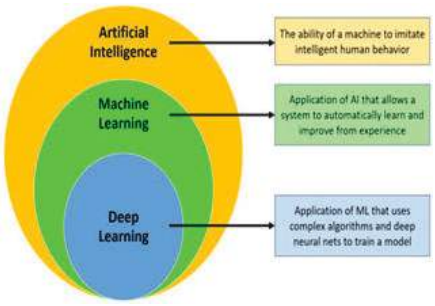

Figure (1): Relationship between AI, ML and DL

Consequently, deep learning is an algorithmically based on the structural and functional organization of the neural model of the human brain, wherein computational mod-

 ISSN: Online 2790-1637, Print 2790-1629
National Library of Libya, Legal number: 154/2018

els can automatically extract, represent, and comprehend the high-dimensional and complex framework that composes large amounts of unstructured visual data [7].

Deep neural networks (DNN) are a form of artificial neural networks (ANN) characterized by a layering of neuron-like processing units, in which each layer produces more abstract feature representations through the nonlinear transformation of inputs. In order to classify images at the input layer, the deep neural network learns from the raw picture data, the pixel intensity value. The input layer learns pixel intensity value, and the hidden layers transform that value through pooling, activation functions, and convolutions to reduce or improve useful, discriminative features and meaningful learning features. Structure and parts develop into higher-level features (ex, shapes) from the low-level features (ex, textures, edges) learned in the first layer to the features learned in the hidden layers. The output layer will relate those higher-level features, low-level features, and potential objects from the predefined categories and give you the final classification. Figure 2 shows the internal structure of both ANN and DNN [8-9].

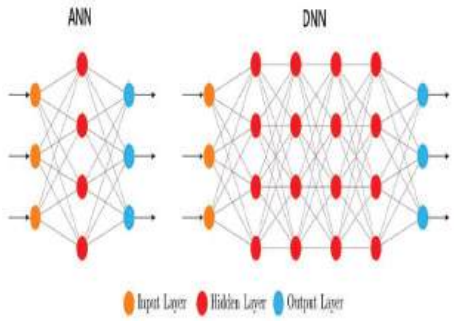

Figure (2): ANN and DNN structure.

In context, convolutional Neural Networks (CNNs) are a subclass of Deep Neural Networks (DNNs) for especially efficient and scalable processing of grid-structured data [10], typically digital image data. CNNs are designed with convolutional layers that can exploit spatial hierarchies of features and are really useful in many application areas in computer vision. The convolutional layer can be thought of as a multi-channel global filter inspired by human vision that is arranged to enter information through areas of special perception that break down the processing requirements of visual stimuli by hierarchically filtering increasingly complex stimuli [11]. A common CNN for image classification is typically built with three layers in mind:

-Convolutional Layer:

This applies a group of filters (kernels) to the image to determine low-level image features such as edges, corners, and textures while maintaining relationships between pixels spatially. A convolution is a mathematical operation that takes two inputs: one is an image matrix, and the other is a kernel or a filter.

-It will process an image matrix of size h × w × d with a filter size of

-The output size will then be, (Figure 3)[12].

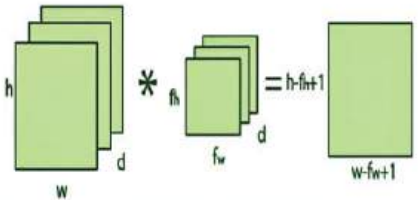

Figure (3): Image matrix multiplies kernel or filter matrix

-Pooling Layer: To decrease feature map spatial dimensions to reduce the computational cost, as well as increase invariance to small translations. Common pooling methods include max pooling and average pooling, (figure 4)[13].

 ISSN: Online 2790-1637, Print 2790-1629
National Library of Libya, Legal number: 154/2018

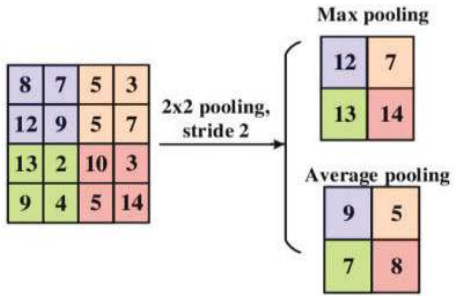

Figure (4): Illustration of max 2×2 pooling with a stride, comparing with the outputs of max pooling and average pooling

-Fully Connected Layer: This layer will flatten the feature maps into a vector and have fully connected (dense) connections to arrive at where we produce the final classification output. In fake note detection, this layer provides the final output probabilities of whether a note is "real" or "fake," applying an activation function such as the SoftMax or sigmoid. As shown in Figure 5, the CNN process converts the feature map matrix into vector representations, joins features, and applies activation functions like SoftMax or sigmoid to classify outputs. This integrated approach allows for robust hierarchical feature representations, crucial in complex visual recognition tasks like counterfeit currency detection [14].

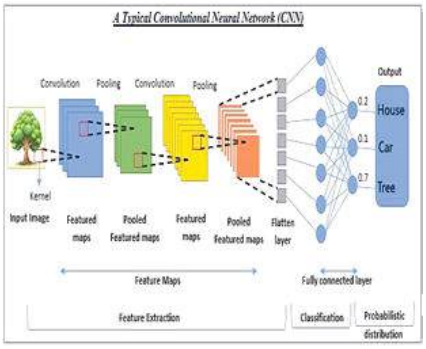

Figure (5): Workflow of convolutional, pooling, and fully connected layers.

1.2.Transfer Learning:

Transfer learning is a method of deep learning that improves model performance on small datasets by reusing knowledge from extensive datasets. This approach overcomes the limitations of deep learning, which often require large volumes of high-quality labeled data, by reusing knowledge from similar tasks with fewer data points [15]. In addition, transfer learning involves freezing initial layers of a pretrained model and retraining later layers to adapt to new domains. Fine-tuning allows for better refinement of task-specific features. Transfer learning offers advantages like shorter training time, better performance on smaller data sets, and lower computational costs, making it suitable for medical image analysis, fraud detection, and counterfeit currency detection. The EfficientNetB4 architecture is chosen for transfer learning [16].EfficientNetB4 is a mid-tier model with advanced accuracy and moderate resource usage cost, pre-trained on the ImageNet dataset. It uses transfer learning to improve classification accuracy and generalization, enhancing automated counterfeit currency detection[17].

1.3. Explainable Deep Learning:

Deep learning has achieved a tremendous level of accuracy on computer vision tasks, yet the advanced complexity of deep neural networks makes them "black boxes", clouding transparency and interpretability. Interpretable AI research also identifies this "black box" characteristic as the most important barrier to actualizing deployments of deep learning in high-stakes domains. As a remedy to this issue, Explainable AI (XAI) techniques have been developed to make model decisions and outcomes more comprehensible [18]. There are a multitude of XAI techniques, and commonly used methods include Gradient-weighted Class Activation Mapping (Grad-CAM) and heatmap visualizations, which can shed light on the inner workings of convolutional neural networks (CNNs) and demonstrate what areas of an image were most pertinent to predicting the final outcome [19].Grad-CAM operates on the premise of utilizing the gradients of class scores for the target class flowing into the last convolutional layers to create a coarse localization map that highlights where in the image is discriminative to the prediction of the model [20]. It allows researchers and

practitioners to observe where the model focuses its attention during classification, creating a kind of interface between high accuracy and the need for interpretability in their use of deep learning[21].

While Grad-CAM is a solid approach to conveying important information, as shown in Figure 6, heatmap visualizations can provide an easy-to-understand color-coded representation of those regions. Warmer colors (e.g., red and orange) indicate areas of high contribution by the model, while cooler colors (e.g., blue) denote areas of lower contribution [22]. In deep learning applications like counterfeit currency detection, heatmap visualizations allow us to grade whether the model is using appropriate security features (e.g., holograms, watermarks, or micro-texts) versus making predictions based on a background that might be incidental [23]. Integrating the predictive capabilities of deep learning methods through Grad-CAM, along with heatmap visualization of decision areas, brings researchers the best of both worlds. It provides the justification of the analytical ability of the assumptions relied upon while conveying the sort of transparency needed for validation and trustworthiness. This combination is not limited to supporting debugging and error analysis; it allows for obtaining evidence for claims, aiding the credibility of AI systems that are deployed in sensitive areas such as finance or security [24].

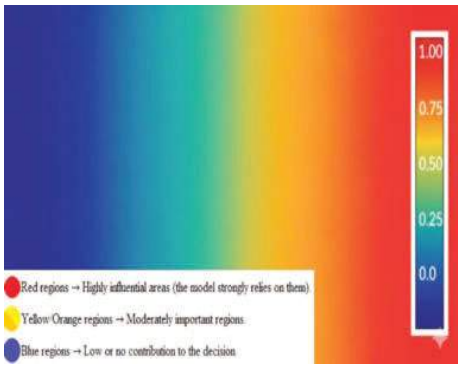

Figure (6): Attention heatmap

1.4. Security features of Libyan banknotes:

The official currency of Libya is the Libyan dinar (LYD). Like most modern currencies, the Central Bank of Libya has developed a range of security features in the banknotes to help avoid counterfeiting and maintain public trust and confidence in the currency system. The securities are the result of an ongoing process of technological innovation and the development of international standards for currency design and authentication. The security features are indicative of both technological and design aspects that serve to maintain the integrity of the national currency. The security design of the Libyan banknote incorporates a number of visible and hidden features that provide protection from counterfeiting and/or demonstrate authenticity. Visible anti-counterfeiting features include, but are not limited to, a dynamic color-shifting 3D holographic stripe, an engraved portrait, and a clear, translucent area, with colored gravure patterns also providing security and attractive visual features. Modern optical features such as optically variable ink (SPARK), fluorescent numbering, and monochromatic serial numbering offer significant layers of authentication in an optical method. Monochromatic serial numbering is identifiable with magnetic properties in order to enable unique identification for automated detection. Raised-intaglio printing can also enhance tactile-based identification and accessibility. An engraved gravure stripe also provides sufficiently micro-level textures that are extremely difficult to reproduce. In this research, an image processing approach and deep learning techniques are used to analyze these features and develop an intelligent system that is able to perform accurate discrimination of genuine Libyan banknotes compared to counterfeits and increase the reliability and automation of currency verification, as shown in Figure 7).

 ISSN: Online 2790-1637, Print 2790-1629
National Library of Libya, Legal number: 154/2018

Figure (7): Basic features of Libyan security banknotes

2. METHODOLOGY

The methodology describes the study approach, data source, preprocessing steps, model design and training, and systematic evaluation procedures. It includes examples of the prototype user interface and system workflow. The systematic procedures ensure that every part of the project contributes to achieving a practical and accurate counterfeit detection system. The study includes statistical and visual performance measures, and the prototype user interface demonstrates how modules fit together in an organized flow. This study uses an applied experimental approach as the goal is to resolve a real-life issue (currency verification) with experimental training and evaluation of deep learning models for image classification, and using transfer learning to help reduce training complexity and resource consumption. EfficientNet-B4, the most current CNN model, was used as the core model due to its balance of accuracy versus computational efficiency.

2.1. System Architecture:

The proposed system employs a modular system where they are self-contained in a self-contained function to deliver the entire workflow. The proposed system in the figure below identifies five mains. The workflow highlights the various key stages planned in the overall design process: image preprocessing, building a CNN using EfficientNet-B4, training the model using the best hyperparameter setups, testing the model with statistical measurements of performance, and developing a prototype graphical user interface (UI) for end-users to interact with. The workflow demonstrates that the proposed system is reproducible, efficient, and scalable. These allow the proposed system to be adaptable for real-world deployment in individual and commercial use, as outlined in the following Figure (8). Research phases the proposed system, outlining five main axes.

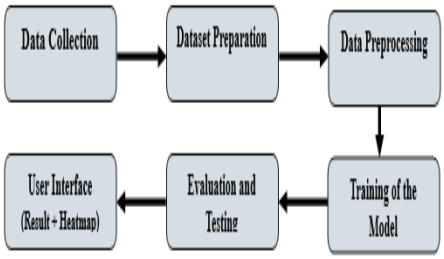

Figure (8): Diagram of the proposed system

2.2. Data Collection

The success of any deep learning system depends primarily on the quality and size of the dataset.

2.2.1. Data Sources:

The Libyan currency will be in denominations of 5, 10, and 20 dinars, and the images are collected from two types of sources:

-Real Currency: Well, provide brand new, clean samples of Libyan banknotes from an established source, preferably a commercial bank.

-Fake Currency: Obviously, obtaining real samples of fake currency is going to be exponentially more difficult, so it is really a case of attempting to simulate fake samples, emulated by digitally altering the images of the original currency to include the common characteristics of failures in the faking process.

2.2.2. Image Acquisition:

To ensure that the model operates under realistic circumstances, many devices and many shooting situations will be adopted to obtain images. Many modern smartphone cameras will be used to vary the lighting conditions (natural, artificial, or dim), shooting angles, shooting distance, and background type. Modern images of banknotes will include a transparent security zone, thus primarily highlighting the background features.

Therefore, images are taken against either a white or black background, completely obscuring this area from the model so that it is distinct from the currency area. Thus, the model avoids this zone.

2.3. Data Preparation:

Data preparation processes, including data splitting and balancing, were used to ensure the reliability of the proposed model effects before using the datasets.

2.3.1. Data Splitting:

The proposed model will undergo rigorous data splitting to prevent overfitting and ensure reliable results. The dataset will be divided into three exclusive subsets, providing evaluation metrics from previously unexplored data, thereby providing an objective and reliable measure of results.

1.Training set: Approximately 70% of the data will come from the training set. Therefore, the model can use this data for parameter learning so that it can be trained.

2.Validation set: There will be approximately 20% of the data being used for the validation set, and the model will make use of this validation set to tune hyperparameters, observe convergence, and control for overfitting.

3.Test set: The remaining 10% will exclusively be used for final evaluation to provide an unbiased estimate of the performance of the model.

2.3.2. Data Balancing:

Class imbalance is a potential issue during the preparation of the dataset. Imbalance leads to bias with regard to the majority class, lowering sensitivity to the minority class. Balancing techniques include oversampling of the minority class, undersampling of the majority classes, or a hybrid of both, to achieve the most appropriate balance without sacrificing data diversity. Allora combination of these will assist in overcoming this limitation found in many real-world applications.

2.3.3. Dataset Description:

This study utilized two datasets for its research purpose: dataset 1 (Currency Verification) and dataset 2 (Authenticity Detection). The first dataset is used to determine if an image is a Libyan banknote, a filtering step before authenticity detection. If the input is not Libyan currency, such as a foreign currency banknote or non-currency image, it is filtered out of the classification pipeline. To make it clear, the division is shown in Table (1) as follows:

Table. (1): Distribution of the image verification dataset

Type of Image	Libyanbanknote	Not a Libyan currency
Total	1000	1000
Training = 70%	700	700
Validation=20%	200	200
Testing = 10%	100	100

Similarly, dataset 2 (Authenticity Detection) is a dataset of banknote images labeled as real or counterfeit, sourced from public and in-person sources. It was used for training and evaluating the model's performance to distinguish real banknotes from fake ones, enabling the model to distinguish between real and counterfeit banknotes. To make it clear, the division is shown in Tables (2) and (3) as follows:

Table. (2): Distribution of the real currency dataset

Type of Currency	20 LYD	10 LYD	5 LYD
Total	1500	1500	1500
Training= 70%	1050	1050	1050
Validation= 20%	300	300	300
Testing= 10%	150	150	150

Table. (3): Distribution of the fake currency dataset

Type of Currency	20 LYD	10 LYD	5 LYD
Total	1500	1500	1500
Training= 70%	1050	1050	1050
Validation= 20%	300	300	300
Testing= 10%	150	150	150

2.3.4. Data Preprocessing

Preprocessing is a significant part of guaranteeing that the input data we use for CNN is consistent, reduces noise, and remains representative. Before we input images into our model, they must have undergone some form of preprocessing to help standardize the images and improve their quality, as illustrated in Figure (9).

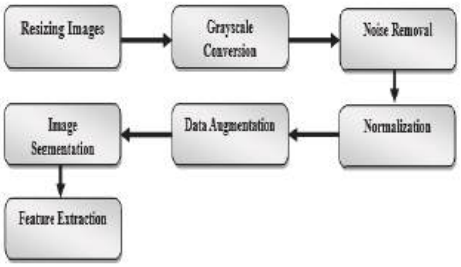

Figure (9): Diagram of data preprocessing operations.

1. Resizing Images: all images should be resized to 380 x 380 pixels to match the input size of EfficientNet-B4.

2. Grayscale Conversion: while the model can handle RGB input, converting to grayscale reduces complexity.

$I_{gray}(x,y)=0.299R+0.587G+0.114B$

3. Noise Removal: A Gaussian filter was used to demean the image:

$$G(x,y) = \frac{1}{2\pi\sigma^2}.e^{\frac{-(x^2+y^2)}{2\sigma^2}}$$

4. Normalization: The pixel values within all images will be scaled from the range [0-255] to the range [0-1]. This operation helps to speed up the model training process and provide a stable range of input. Pixel intensities were normalized to the range [0,1]

$$x' = \frac{x - min(x)}{max(x) - min(x)}$$

5. Data Augmentation: To synthetically enlarge the number of members and diversity in the dataset, random changes will be made to the images, which could include adding minor rotations, zooming in and out, and changing brightness. Random changes were used to enrich dataset variability: rotation (θ), zoom, brightness, and flips.

6.Image Segmentation: The study utilizes the Squeeze-and-Excitation (SE) Block for channel-wise feature recalibration in computer vision, enhancing robust segmentation and feature extraction in challenging situations. Figure (10) depicts the general scheme of the suggested segmentation.

(1). Holographic Stripe. (2). Protection. Portrait, Clear Window. (3). SPARK on Secondary Window. (4). Magnetic numbering. (5). Fluorescent numbering. (6). Tactile Emboss. (7). engraved Gravure stripe. (8). Relief writing. (9). The prominent engraved landmark. (10). The signature

Figure (10): Basic features of data Libyan security banknotes.

7. Feature Extraction Segmented regions are converted into numerical descriptors for machine learning models through a process known as feature extraction. Conventional techniques use features like texture or color histograms and modify them according to their dependability. Deep learning approaches, such as CNN models, with attention strategies like the Squeeze-and-Excitation (SE) Block, however, provide more reliable modifications, enabling networks to improve classification performance by increasing informative capabilities and decreasing uninformative ones. A summary of preprocessing methods and their benefits is shown in Table (4).

Table (4): Image preprocessing methods and benefits

Technique	Purpose	Effect
Resizing (380×380)	Uniform input for CNN	Standardization
Grayscale Conversion	Reduce computational cost	Simplicity
Gaussian Filtering	Reduce noise	Clarity
Normalization [0,1]	Improve convergence speed	Stability
Data Augmentation	Increase dataset size, reduce overfitting	Robustness
Image Segmentation	Highlight discriminative regions	Feature Enhancement

Table (4) outlines image preprocessing steps for CNNs, including resizing, grayscale conversion, Gaussian filtering, normalizing data to [0,1], and data augmentation and segmentation for robustness and discrimination among classes.

The pseudocode describing the preprocessing and augmentation pipeline is showed in Figure (11).

```
preprocess_pipeline = Preprocessing)
   resize‹(380 ‹380) =
   grayscale = True‹
gaussian_filter = {kernel_size: ‹{1.0 :amgis ‹5
   normalization‹[1 ‹0] =
   augmentation} =
      rotation: ‹±7
zoom_range: ‹1.1
      brightness: {alpha: {10 :ateb ‹1.1
‹{
   segmentation} =
otsu_threshold: True‹
adaptive_threshold: {block_size: {2 :C ‹31
{
(
```

Figure (11): Pseudocode for data preprocessing and augmentation pipeline.

2.4. Model Development and Training:

This is the important part of the investigation where we will be building the "brain" of the system.

2.4.1. Model Selection:

At the heart of the system, we are using a convolutional neural network (CNN). In order to accelerate the development process of the system and take advantage of the availability of powerful models trained on millions of images, we will follow a transfer learning approach. The model we have proposed to use is EfficientNet-B4 because of its high efficiency coupled with a small footprint, which we favor for future use in a smartphone application. EfficientNet-B4 is an efficient trade-off. It also uses a compound scaling process that jointly scales depth (d), width (w), and resolution (r):

$$d = \alpha^{\varphi}, w = \beta^{\varphi}, r = \gamma^{\varphi}$$

where φ is the scaling coefficient, and constants were selected from a grid search in a constrained resource relative to α, β, and γ.

2.4.2. Modified architecture for binary classification:

A pre-trained EfficientNet-B4 (trained on ImageNet) was used as a feature extractor, and a dropout layer and a final sigmoid output were added. The architecture is shown in Figure (12), The top layers were replaced by custom dense layers.

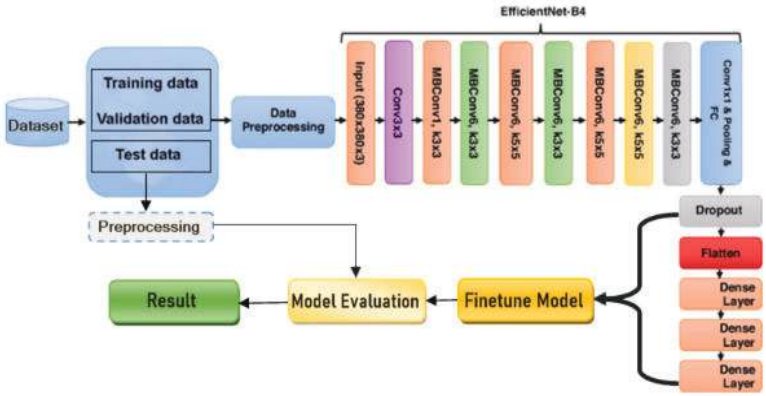

Figure (12): CNN model architecture (EfficientNet-B4 Modified for binary classification)

 ISSN: Online 2790-1637, Print 2790-1629
National Library of Libya, Legal number: 154/2018

2.4.3. Training Process:

-Loss Function: The loss function that will be used is binary cross-entropy, which is the most commonly used loss function for binary classification problems. Binary cross-entropy was used:

$$L = -\left(\frac{1}{N}\right) \Sigma \left[y_i \log(\hat{y}_i) + (1 - y_i) \log(1 - \hat{y}_i) \right]$$

-Optimizer: The optimizer we will use is the Adam optimizer, because of the ability of the Adam optimizer to converge fast. Adam updates stage parameters with:

-First moment estimation : $mt = \beta^1 mt^{-1} + (1 - \beta^1) gt$

-Second moment estimation : $vt = \beta^2 vt^{-1} + (1 - \beta^2) gt^2$

-First trend bias correction: $\hat{m}_t = \frac{mt}{1 - \beta_1^t}$

-Second – direction bias correction:

$$\hat{v}t = \frac{vt}{1 - \beta^{2t}}$$

Base update: $\theta_{t+1} = \theta t - \frac{\alpha \hat{m} t}{\sqrt{\hat{v}t} + \varepsilon}$

AdamW improves generalization on vision models by decoupling weight decay from the gradient update.

-Performance Metrics: Accuracy will be primarily monitored during training.

-Hyperparameters: The table (5) indicates that the configurations for the training set were based on a Batch Size of 32, as this achieved a balance of stability and computational efficiencies, and 30 Epochs, which allowed ample learning to occur and to mitigate overfitting. The Adam optimizer was selected for quicker convergence, and to ensure stable updates, while Binary Cross-Entropy was selected as the loss function, given that the task is a binary classification task.

Table (5): Training hyperparameters

Parameter	Value
Batch Size	32
Epochs	30
Optimizer	Adam
Loss Function	Binary Cross-Entropy

2.5. Model Evaluation

To assess the model's efficacy, a suite of performance indicators based on the confusion matrix will be deployed after assessing the model on the test dataset.

1.Accuracy: The portion of correct classifications over total samples.

$$Accuracy = \frac{TP + TN}{TP + TN + FP + FN}$$

Where TP: True Positi.

FP: False Positive

TN: True Negative.

FN: False Negative.

2.Precision: Of all of the banknotes that the model classified as "Fake", what percentages were correct? (It was possible).

$$Precision = \frac{TP}{TP + FP}$$

3.Recall/Sensitivity: Of all the real "fake" banknotes, what percentage did the model detect? (It was important that no counterfeit coins were missed).

$$Recall = \frac{TP}{TP + FN}$$

4.F1-Score: The harmonic mean between precision and recall, it is an overall indicator of a model's performance.

$$F1 = 2 . \frac{Precision\ Recall}{Precision + Recall}$$

5.Confusion Matrix:

Table (6) shows the confusion matrix parameters used to evaluate the performance of the proposed deep learning model, including true positive (TP), false positive (FP), true negative (TN), and false negative (FN). These metrics form the basis for calculating accuracy, precision,

recall, and F1 score.

Table (6): Confusion matrix parameters

		Actual	
		Real	Fake
Predicted	Real	TP	FP
	Fake	FN	TN

TP=∑(ytrue=1 ∧ ypred=1)

FP=∑(ytrue=0 ∧ ypred=1)

TN=∑(ytrue=0 ∧ ypred=0)

FN=∑(ytrue=1 ∧ ypred=0)

Where,

-True Positive (TP) is an image that is labeled with an Original Banknote that is predicted as a Real Banknote.

-False Positive (FP) is an image ed as "Fake Banknote" that is predicted as " Real Banknote."

-False Negative (FN) is an image labeled with a Real Banknote that is predicted as a Fake Banknote.

-True Negative (TN) is an image labeled with "Fake Banknote" that is predicted as a Fake banknote.

6. ROC and AUC

To evaluate the efficacy of the proposed CNN-based banknote authentication system further, Receiver Operating Characteristic (ROC) curves were employed. Receiver Operating Characteristic (ROC) Curve: A ROC curve is a graphical representation that shows the trade-off between True Positive Rate (TPR, also called Recall or Sensitivity) and False Positive Rate (FPR) at multiple

$$TPR = \frac{TP}{TP + FN} \quad FPR = \frac{FP}{FP + TN}$$

In the ROC plot:

• X-axis (FPR): Proportion of real banknotes classified incorrectly as counterfeit.

• Y-axis (TPR): Proportion of counterfeit banknotes correctly classified as counterfeit

6.1.Area Under the Curve (AUC):

The AUC is a single scalar that summarizes the classifier's performance at all thresholds. The AUC is the area under the ROC curve. AUC values are in the range of [0, 1]:

$$AUC = \int_{[0,1]} TPR(FPR)\, d(FPR)$$

AUC value interpretation:

• AUC = 1.0 → Perfect classifier (best case)

• 0.9 ≤ AUC < 1.0 → Excellent classification performance

• 0.8 ≤ AUC < 0.9 → Good classification performance

• 0.7 ≤ AUC < 0.8 → Acceptable classification performance

• 0.5 ≤ AUC < 0.7 → Poor classification performance (similar to random guessing)

• AUC = 0.5 → model has performance equivalent to random chance

• 0.5 ≤ AUC < 0.7 → Poor classification performance (similar to random guessing)

• AUC = 0.5 → The model has performance equivalent to random chance.

ROC curves allow a greater degree of scrutiny of the classifier beyond a simple number of overall accuracy measures. In the counterfeiting realm of banknote detection:

• A high TPR means fakes will not be missed.

• A low FPR means real banknotes will not be marked as fake.

Thus, the ROC-AUC analysis provides a reasonable balance between the model's ability to be sensitive to counterfeit notes and its integrity in marking real notes.

6.2.User Interface Design (Prototype)

A prototype user interface will be developed using the Tkinter library in Python in order to create a straightforward method of utilizing the proposed model. The user interface will be preliminary and scalable in the future. The user will be able to upload a photo from their studio or take one directly from their camera and pass it to the model to make a prediction on the currency denomination (genuine or counterfeit). The user interface will also include an additional button to show a heatmap, the focus areas, which show the decision-making focus areas, and would further improve interpretability. The prototype is not the final destination; it is the start of the process that allows one to develop a fully integrated user interface

 ISSN: Online 2790-1637, Print 2790-1629
National Library of Libya, Legal number: 154/2018

for an eventual commercial or institutional effort. The prototype was created using Tkinter. The main system interface, as shown in Figure 13, is as follows:

Figure (13): Main operational interface of the Libyan currency detector

6.2.1.Functional Components

Table 7 shows the most important components of the system and their functions.

Table (7): Functional Components

Component	Function
Select Images	The user can upload an image of Libyan currency to be verified.
Predict	The system will then use the pre-trained deep learning model to predict if the currency is real or fake.
Heatmap	The user can visualize the saliency/heatmap that displays the most salient regions in the model's class label decision; this will allow the user to have explainable AI.
Clear	The current image and results from this previous prediction are removed, enabling the user to start over.
Camera	The user is able to capture an image for immediate verification.
Exit	The user can exit the application.
Previous/Next	Allows you to navigate through multiple uploaded images.
Result section	Shows the output of the prediction and initially prompts the user to select an image before producing any results.

2.7. Workflow Flowchart:

To better visualize the sequential operations of the system, a workflow flowchart was developed. It outlines the steps from image acquisition to classification. The pipeline includes image-preprocessing, augmentation, model training, and evaluation, as illustrated in Figure 14. The workflow integrates all modules:

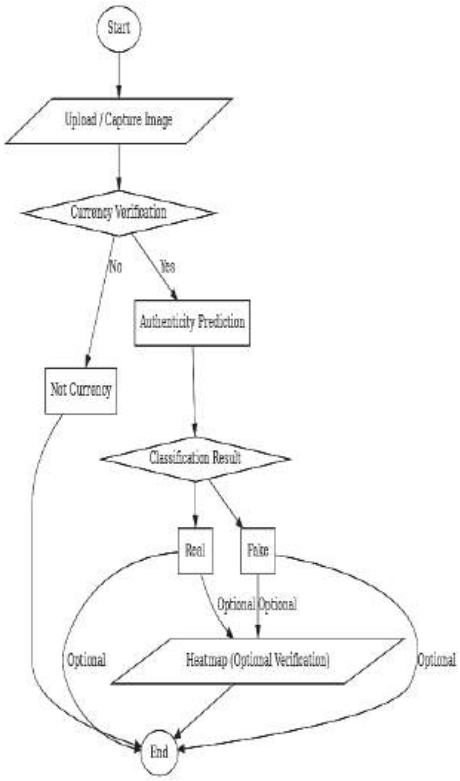

Figure (14): Flowchart of the complete system

2.8. Tools and Techniques Used

2.8.1. Hardware Specification:

Table 8 shows the hardware specifications used in implementing and evaluating the proposed system.

Table (8): Hardware Specification

Component	Specification
Processor	Intel i3 2GHz
RAM	4 GB
Storage	512 GB HDD

2.8.2. Software Specification:

Table 9 presents the software specifications employed in the development and testing of the proposed system.

Table (9): Software Specification

Software	Specification
Operating System	Windows 10
Programming Language	Python 3.10
IDE (Integrated Development Environment)	VS Code
Libraries	TensorFlow, Keras, OpenCV, Scikit-learn, Numpy, Pandas, Seaborn
Model training environment	Google Colaboratory
Storing and managing data	Google Drive (cloud storage)

3.RESULTS AND EVALUATION

3.1. Model 1: Currency VS. Not Currency:

The first stage required classifying if a banknote image belonged to Libyan currency or not. The EfficientNet-B4 model was trained and evaluated on Dataset 1. The EfficientNet model has a compound scaling and optimized architecture, which aided in high levels of accuracy when detecting Libyan banknotes. The model's overall performance, evaluated based on performance measures, is synthesized below:

3.1.1. Training Performance:

Figure 15 (Training Performance) shows the change in accuracy and loss during the training process. It can be seen that the model performance improved significantly from the outset (after 0 epochs) with training accuracy increasing to 100% and training loss (1.1565e-04) and a validation accuracy of 98.76% after the 5th epoch. From that time onwards performance stabilization occurred, and performance was maintained at a high-performance level for both groups of subjects. In relation to the loss—

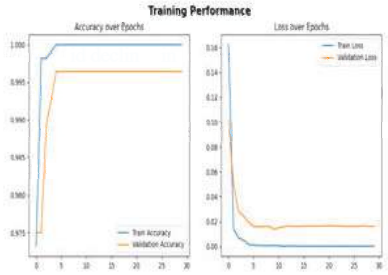

Figure (15): Training & validation accuracy and loss curves for Model 1

3.1.2. Confusion Matrix:

Figure 16 and Table 10 provide the confusion matrix, which indicates the model was able to correctly classify all samples at 100%. Therefore, the model correctly identified both currency and non-currency without any false positives or false negatives. The results show that the model was distinguished between the two categories effectively and has shown the ability to generalize well.

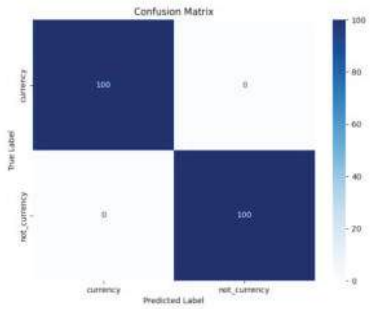

Figure (16): Confusion matrixfor Model 1

Table (10): Confusion Matrix Results for Model 1

		Actual	
		Real	Fake
Predicted	Currency	TP= 100	FP= 0
	Not Currency	FN= 0	TN= 100

3.1.3. Performanc Metrics:

The model highlighted in Table 11 demonstrated accuracy equal to 100% for each of the four performance statistics of accuracy, precision, recall, and F1 rate. The model with zero error was able to classify the samples into currency and non-currency classes with no class error and indicated high class discrimination ability. All total averages (Macro Avg + Weighted Avg) were also equal to 100% accuracy, which indicated the model achieved strict accuracy across the entire data set. These values were calculated from Table 10 stemming from the confusion matrix.

$$Accuracy = \frac{TP + TN}{TP + TN + FP + FN} = \frac{100 + 100}{100 + 100 + 0 + 0} = 1.0(100\%)$$

$$Precision = \frac{TP}{TP + FP} = \frac{100}{100 + 0} = 1.0(100\%)$$

 ISSN: Online 2790-1637, Print 2790-1629
National Library of Libya, Legal number: 154/2018

$$Recall = \frac{TP}{TP + FN} = \frac{100}{100 + 0} = 1.0(100\%)$$

$$F1 = 2 . \frac{Precision . Recall}{Precision + Recall} = 2 . \frac{1.0}{1.0 + 1.0} = 1.0(100\%)$$

Table (11): Performance metrics for Model 1

Class	Precision	Recall	F1-score	Support
Currency	1.00	1.00	1.00	100
Not Currency	1.00	1.00	1.00	100
Accuracy			1.00	200
Macro Avg	1.00	1.00	1.00	200
Weighted Avg	1.00	1.00	1.00	200

3.1.4. ROC Curve and AUC Analysis:

The ROC curve in Figure 17 extends the illustration of the model's performance in class discrimination appropriately, as the AUC (area under the curve) reached its maximum value of 1.0, signifying perfect classification performance with no classified error. The blue line has shown that the true positive rate (TPR) was continually high across all false positive rates, which suggests that the model's strength was in being able to optimally balance sensitivity and specificity. TPR and FPR calculated as:

$$TPR = \frac{TP}{TP + FN} = \frac{100}{100 + 0} = 1.0\ (100\%)$$

$$FPR = \frac{FP}{FP + TN} = \frac{0}{0 + 100} = 0$$

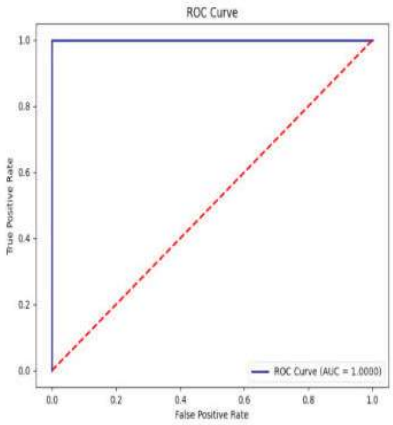

Figure (17): ROC Curve& AUC for Model 1

3.2. Model 2: Real VS. Fake Classification

3.2.1. Training Performance for Model 2:

Figure (18) presents the training and validation performance metrics from the proposed model as it was supplied with genuine and counterfeit currency. The left plot shows the accuracy plots over several training epochs, where it was clear that the training accuracy climbed steadily to nearly 90% while the validation accuracy settled downwards at 88%. This would imply that the model generalizes well and there was no blatant overfitting. The right plot presents the loss values for training and validation. Here, the training loss fell steadily below 0.25, and the validation loss settled down at approximately 0.30 after about the fifteenth epoch, which shows that the model was still learning. Overall, the take-home message was that the model can distinguish between genuine currency and counterfeit currency reliably after only a number of training epochs, and it has also demonstrated strong and consistent performance in doing so.

 ISSN: Online 2790-1637, Print 2790-1629
National Library of Libya, Legal number: 154/2018

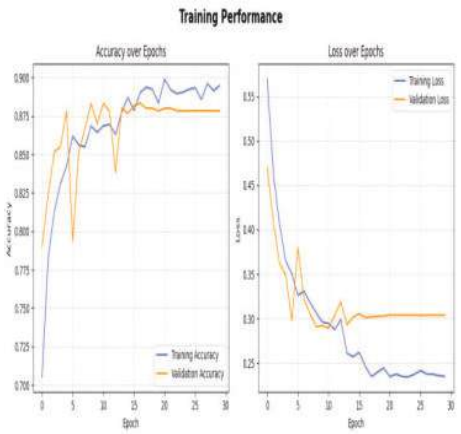

Figure (18): Training & validation accuracy and loss curves for Model 2

3.2.2. Confusion matrixfor model 2:

Figure (19) and Table (12) the confusion matrix incorporates the measures of performance for the proposed model tested on the test dataset, including 150 genuine samples and 150 counterfeit samples. The model had correctly classified 141 genuine notes; meanwhile, there were 142 counterfeit notes being correctly classified as the positive tie. This also corresponded with the model misclassifying only nine genuine notes as counterfeit, while misclassifying eight counterfeit notes as genuine notes. Overall, these results suggest that the model is quite robust in categorizing real from fake currency, as well as the high level of precision/recall for both classes. The lower count of misclassifications implies strong reliability and that this model can be practically applied to real-world applications that identify counterfeit currency.

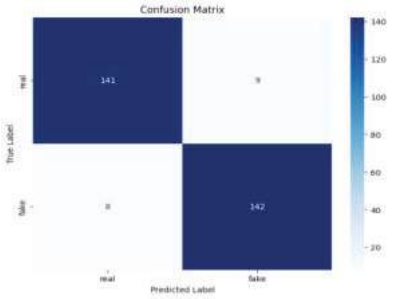

Figure (19): Confusion matrixfor Model 2

Table (12): Confusion Matrix Results for Model 2

		Actual	
		Real	Fake
Predicted	Real	TP= 141	FP= 9
	Fake	FN= 8	TN= 142

3.2.3. Performance metrics for model 2:

The confusion matrix describes the success of the proposed model on the test dataset of 300 samples (150 real and 150 fake). As indicated by the confusion matrix, the model successfully predicted 141 real notes and 142 fake notes with only (9 + 8 = 17) misclassifications, as shown in Table 13. Using the proposed model's results, the evaluation metrics were calculated as:

$$Accuracy = \frac{TP + TN}{TP + TN + FP + FN} = \frac{141 + 142}{141 + 142 + 9 + 8} = 0.943$$

$$Precision = \frac{TP}{TP + FP} = \frac{141}{141 + 8} = 0.9463$$

$$Recall = \frac{TP}{TP + FN} = \frac{141}{141 + 9} = 0.9400$$

$$F1 = 2.\frac{Precision.Recall}{Precision + Recall} = 2.\frac{0.8905}{1.8863} = 0.9431$$

The abovementioned results have demonstrated that the model had an overall accuracy of 94.33% with equal precision and recall in both classes; it presented the potential to accurately detect authentic versus counterfeit currency.

3.2.4. ROC Curve Analysis:

The ROC shows the relationship between TPR (True Positive Rate) and FPR (False Positive Rate) of the proposed model that the confusion matrix results yielded, with TPR calculated as:

Table (13): Performance metrics for Model 2

Class	Precision	Recall	F1-score	Support
Real	0.9463	0.9400	0.9431	150
Fake	0.9404	0.9467	0.9435	150
Accuracy			0.9433	300
Macro Avg	0.9434	0.9433	0.9433	300
Weighted Avg	0.9434	0.9433	0.9433	300

$$TPR = \frac{TP}{TP + FN} = \frac{141}{141 + 8} = 0.9493$$

Moreover, FPR calculated as:

$$FPR = \frac{FP}{FP + TN} = \frac{9}{9 + 142} = 0{,}0596$$

As seen on the ROC curve (Figure 20), the model continued to demonstrate an extremely strong separation of real versus fake classes, as evidenced by the AUC of 0.9493. This also provided reassurance of the capacity of the model to clearly delineate classes, as when the AUC values are close to 1.0, this means correspondingly few false positives occur, and there was quite a bit of classification capability in the model.

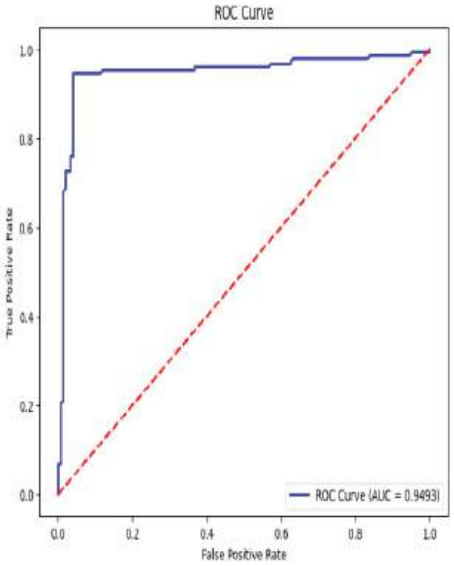

Figure (20): ROC Curve& AUC for Model 2

While the developed model resulted in a reasonable classification accuracy of approximately 94%, this amount did not reach a 100% perfect score based on various technical and transfer factors, which are discussed below. Initially, it could not reach maximum accuracy and performance curves due to several factors related to the data composition and the complex nature of the new Libyan banknote.

The training images were different in aspects of lighting, resolution, and capture angles and had polymer substrate-induced reflections, which made the fine details less clear and caused distortion. Also, the new banknote has security features that are highly complex, including a transparent window, a holographic stripe with a 3D component, and SPARK technology with variable reflectance. These attributes produce dynamic visual patterns that models simply cannot learn consistently. Also, an inconsistent ratio of genuine to counterfeit banknotes can skew the learning and subsequently impact the AUC value.

In contrast, some authors using controlled data with fixed angles and constant illumination reported accuracy as high as 100%, such as [25] on Colombian currency

using ResNet18. For studies with real and variable data, accuracy ranged from 85% to 94%, such as the results of [26] using Jordanian currency. The position of the result in this study is attributed to the fact that modern Libyan polymer banknotes contain transparent areas and three-dimensional elements, as noted by [27], which add complexity by acting as optical elements. Furthermore, under realistic data capture conditions, variation typically reduces generalization only slightly compared to controlled data, as noted by [28]. Overall, achieving around 94% accuracy is commendable and realistic and indicates the existing structural and optical complexity of modern polymer banknotes and the difficulty of producing a complete model of all their security features in a learning framework.

3.3.User Interface Evaluation:

The user interface of the proposed system was constructed with ease of use and ease of operation in mind. As shown in the Figures 21, we used an interface that allows the users to upload images, predict, and return the results without excessive barriers. For example, the system accurately reported that the uploaded image was not Libyan currency and presented a clear, simple error.

This feedback facilitates ease of use by helping the user operate effectively without misleading the user into bad interactions with the system. For Libyan banknotes, the system will tell you whether your inputs are genuine or counterfeit, along with the confidence attached to the prediction. For example, if the prediction results show 90%, the banknote is expected to be either genuine (or counterfeit, depending on the denomination). However, a confidence score of 70% does not simply mean belief that the banknote is “70% counterfeit”; it simply is a measure of the probability of the banknote belonging to the denomination that was predicted. This probabilistic feedback is important for transparency purposes and can help the user make their decisions with more confidence when operating the system.

Figure (21): Screenshot of prediction operations for a Libyan banknote

3.4 .Grad-CAM Heatmap Visualization:

Grad-CAM heat maps were produced for each sample. Visual features of the banknotes from Libya (logo, product's color, design, etc.) were also significant.

The conditions of interpretation are analysis and are through any distributions of suspicious areas. In Figure 22, warm colors (red and yellow) represent the areas enhanced for the end user, add value to the banknotes that had the most amount of influence on predicting the outcome, and cool colors (blue and purple) represent negative influence. This method of interpretation increases the transparency of the model since they can see what the most essential features of the banknotes were in relation to classification, ultimately adding greater reliability and confidence in the detection framework being proposed.

 ISSN: Online 2790-1637, Print 2790-1629
National Library of Libya, Legal number: 154/2018

Figure (22): Screenshots of a Heatmap of a Libyan Banknote

4.CONCLUSION

In conclusion, this study achieved its aim by developing an effective, as well as understandable, deep learning model for counterfeit banknote detection. The study based its contributions on principles from the EfficientNet-B4, the Grad-CAM visualization approach, and a basic prototype user interface to offer practical and technical contributions. While the study has a few notable limitations regarding the dataset and real-world data, the research provides a strong base for future work to build from and extend the work spawned from the study. Thus, this research not only contributes to the academic conversation of deep learning and fraud detection but also provides a direction for practice in the financial and commercial world. In future work, several potential research directions will enhance and expand the scope of the work presented in this paper. Expanding the dataset will ensure the highest possible system accuracy for developers. Furthermore, improving the user experience/UI of both mobile and web applications will create a cross-platform experience.

REFERENCES

1.Barbosa J, Martins H S R, da Silva A J S, NoratoH M G, Duarte, A R. Counterfeit banknote identification based on outlier detection methods. International Journal of Scientific Management and Tourism, 2024;10(2), 45–59. ISSN: 2386-8570.

2.Antonius F, Ramu J, Sasikala P, Sekhar JC, Mary S C. Deep Cyber Detect: Hybrid AI for Counterfeit Currency Detection with GAN-CNN-RNN using African Buffalo Optimization. International Journal of Advanced Computer Science and Applications, 2023;14(7).

3.Alshorman O, Omar K, Ahmad T. Banknotes counterfeit detection using convolutional neural networks with attention mechanisms: A case study on Jordanian currency. Journal of Imaging, 2024 ;10(2).

4.Pham T D, Lee Y W, Park C, Park K R. Deep Learning-Based Detection of Fake Multinational Banknotes in a Cross-Dataset Environment Utilizing Smartphone Cameras for Assisting Visually Impaired Individuals. Mathematics, 2022;10(9), 1616.

5.Van der Horst F, Snell J, Theeuwes J. Finding counterfeited banknotes: the roles of vision and touch. Cognitive Research: Principles and Implications,2020; 5, Article 40.

6.Alzubaidi L, Zhang J, Humaidi A J.. Review of deep learning: concepts, CNN architectures, challenges, applications, future directions. J Big Data, 2021; 8, 53.

7.LeCun Y, Bengio Y. Hinton G. Deep learning. Nature, 2015; 521, 436–444 .

8.Waseem R, Zenghui W. Deep Convolutional Neural Networks for Image Classification: A Comprehensive Review. Neural Comput 2017; 29 (9): 2352–2449.

9.Krizhevsky A, Sutskever I, Hinton G. ImageNet classification with deep convolutional neural networks. In Proc. Advances in Neural Information Processing Systems, 2012; 25 1090–1098.

10.Gupta R., Singh S. Revolutionizing convolutional neural networks for enhanced currency security and fraud prevention. BPAS Journals. 2024; Vol.44 No. 3. P. 24900-24908.

11.Rangel C. A. survey on convolutional neural networks and their performance limitations in image recognition tasks. Journal of Sensors, 2024; 2797320.

O'Shea K, Nash R. An Introduction to Convolutional Neural Networks.2015; ArXiv, abs/1511.08458.

12.Albawi S, Mohammed T A,Al-Zawi S. "Understanding of a convolutional neural network," 2017 International Conference on Engineering and Technology (ICET), Antalya, Turkey, 2017, pp. 1-6, doi: 10.1109/ICEngTechnol.2017.8308186.

13.Ali T, Jan S, Alkhodre A, Nauman M, Amin M, Siddiqui MS. DeepMoney: counterfeit money detection using generative adversarial networks. PeerJ Comput Sci. 2019;5:e216.

14.Wang J, Perez L,Hays J. The effectiveness of data augmentation in image classification using deep learning. Convolutional Neural Networks in Image Processing,2020; 10(4), 450–460.

15.Zhang B, Chen L, Liu X, Zhao L. Practices and challenges of using GitHub Copilot: An empirical study. arXiv preprint arXiv, 2023; 2303.08733.

16.Tan M, Le Q. EfficientNet: Rethinking Model Scaling for Convolutional Neural Networks. In Proceedings of the 36th International Conference on Machine Learning 2019 ;(Vol. 97, pp. 6105–6114). PMLR.

17.Longo L, Lapuschkin S, Seifert C. (Eds.).. Explainable Artificial Intelligence: Second World Conference, xAI 2024, Valletta, Malta, July, Proceedings, Part IV (Communications in Computer and Information Science, 2024;Vol. 2156).

18.Cheng Z, Wu Y, Li Y, Cai L, Ihnaini B . A Comprehensive Review of Explainable Artificial Intelligence (XAI) in Computer Vision. Sensors, 2025; 25(13), 4166.

19.Zhang H, Ogasawara K. Grad-CAM-Based Explainable Artificial Intelligence Related to Medical Text Processing. Bioengineering (Basel). 2023; 10(9):1070. Published 2023 Sep 10.

20.Chattopadhay A, Sarkar A, Howlader P, BalasubramanianV N. Grad-CAM++: Generalized gradient-based visual explanations for deep convolutional networks. IEEE Winter Conference on Applications of Computer Vision (WACV), 2018;839–847.

21.Chefer H, Gur S, Wolf L. Transformer interpretability beyond attention visualization. Proceedings of the IEEE/CVF Conference on Computer Vision and Pattern Recognition (CVPR),2021; 782–791.

22.Samek W.Wiegand T.Müller K. "Explainable Artificial Intelligence: Understanding, Visualizing and Interpreting Deep Learning Models." ArXiv abs/1708.08296 2017: n. pag.

23.Selvaraju R. Cogswell M A, Das R. Vedantam D. BatraD. "Grad-CAM: Visual Explanations from Deep Networks via Gradient-Based Localization,; IEEE International Conference on Computer Vision (ICCV), Venice, Italy, 2017; pp. 618-626, doi: 10.1109/ICCV.2017.74.

24.Pachón, C G, Ballesteros, D M, Renza, D.. Fake banknote recognition using deep learning. Applied Sciences, 2021; 11(3), 1281.

25.Nasayreh A, Jaradat A S, Gharaibeh H, Dawaghreh W, Al Mamlook R M, Al-Na'amneh Q, Daoud M, Migdady H, Abualigah L. Jordanian banknote data recognition: A CNN-based approach with attention mechanism. Journal of King Saud University – Computer and Information Sciences, 2024; 36(4), 102038.

26.Rafiei A, Karimi A, Bodaghi M. Polymer banknotes: A review of materials, design, and printing. Sustainability, 2023; 15(4), 3736.

27.Lee J W. A survey on banknote recognition methods by various sensors. Sensors, 2017;17(11), 2627.

Scientific Journal of University of Benghazi

SJUOB (2025) 38 (2) Applied Sciences: Bashasha. et . al, 94 – 102
www.sjuob.uob.edu.ly

First Karyotype Report of *Arum cyrenaicum* Hruby (Araceae) from AL-Jabal AL-Akhdar, Libya.

Jamila A. Bashasha [1]*, Yousif F. Imryed[1], Halima J. Adam[2]

1. Department of Horticulture, Faculty of Agriculture, University of Benghazi, Libya.

2. Department of Botany, Faculty of Arts and Science-Almarj, University of Benghazi, Libya.

DOI: 10.37376/sjuob.v38i2 | Received:20/09/2025 | Accepted:28/11/2025 | Publishing: 23/12/2025

ABSTRACT

In this paper, somatic chromosome number and karyotype of the endemic species *Arum cyrenaicum* Hruby (Araceae), collected from the Tolmitha site in the Al-Jabal Al-Akhdar region of Libya, are reported for the first time. Our results revealed that all the studied populations were polyploid (2n=4x=56) with a karyotype formula (KF) of 6M+38m+10sm+2st(2SAT). Furthermore, the chromosome size of *A. cyrenaicum* was medium to small-sized, with lengths ranging from the largest 4.72±.21µm to the smallest 2.88±.04µm. According to Stebbins' karyotype asymmetry classification, it was 1A type (symmetrical one). Satellites were observed on two chromosome pairs. The karyotypes of these species' findings contribute to the scientific understanding of this plant from a genetic perspective study. In addition to taxonomic characters, the analyzed karyotype features will contribute to the characterization of *A. cyrenaicum* varieties and to establish a base for future research.

KEYWORDS: Chromosome numbers, karyotype, endemic, *Arum cyrenaicum*.

Corresponding Author: Jamila A. Bashasha.

 ISSN: Online 2790-1637, Print 2790-1629
National Library of Libya, Legal number: 154/2018

1.INTRODUCTION

Araceae is a large plant family that comprises 140 genera and about 4,075 known species[1] . In Libya, there are 3 genera and 3 species: 1. Arum 2. Biarum 3. Arisarum [2]. *Arum cyrenaicum* (vernacular name: Renish) is an annual herbaceous plant with discoid-shaped tubers, which grows during the early fall season. It has simple sagittate and hastate leaves with long petioles (Fig. 1). The species produces a single inflorescence, which is sail-shaped and dark purple in color. The inflorescence consists of two parts: the spathe and the spadix, blooms during March-April. The fruits of *A. cyrenaicum* are red berries when ripe, and the seeds have an ovate shape[3]. Traditionally, *A. cyrenaicum* has been used in Libyan folk medicine for treating dermatitis, psoriasis, diarrhea, and diabetes[4,5]. Phyto-chemical studies have revealed the presence of flavonoids, alkaloids, terpenes, carbohydrates, and sterols [6]. *A. cyrenaicum* was first described as a Libyan endemic species by Hruby [7], was previously misclassified under multiple names. Initially, Durand and Barratte [8] identified it as A. hygrophilum. Later, in 1910, the same researchers referred to it as Arum italicum, while Pampanini [9] assigned it the name *Arum pictum.*

Plant karyotype study is fundamental for understanding the origin and evolutionary pathways of plant species, as well as contributing to molecular genetics and floristic geography [10]. In addition, karyotype research is a fast, inexpensive approach to classify plant species by identifying the basic cytological parameters of a species, including chromosome number, size, morphology, ploidy levels, and karyotype coefficient of variation [11]. These characteristics are considered vital sources of taxonomic information, as they serve as powerful tools for the authentication and identification of
plant species after morphological studies [12].

Although modern biosystematics relies heavily on molecular approaches, karyological data remain indispensable for understanding genome organization and evolutionary diversification [13].

The genus Arum comprises both diploid (2n = 28) and polyploid taxa (2n = 56 and 84), with polyploidy playing a role in species diversification and adaptation [14]. The basic chromosome number for Arum is x = 14, and species exhibit significant variation in karyotype morphology and asymmetry [15].

D'Emerico et al. [16] studied chromosome morphology in five species of the genus Arum . Their results showed that the karyotypes of A. orientale, A. alpinum, and A. nigrum (2n = 28) were very similar. A. pictum (2n = 28) is composed of a higher number of asymmetric chromosomes. The karyotype of A. maculatum (2n =56) shows great similarities to the karyotypes of A. orientale and A. alpinum.

Some studies have shown that certain Arum species share similarities in their morphological karyotype characteristics. A. italicum and A. maculatum share a similar karyotype morphology. On the other hand, A. italicum, with a higher intra-chromosomal asymmetry index (A1 = 0.43), exhibits a more asymmetrical karyotype than A. maculatum (A1 = 0.39). In comparison to A. maculatum and A. italicum, A. apulum (A1 = 0.32) has the most symmetrical karyotype [15]. According to reports, the majority of polyploid Arum taxa cover larger geographic areas than their diploid counterparts [17]. A. italicum is found throughout the Mediterranean region, the Atlantic coast, and the Caucasus [18]. Central and Western Europe are home to A. maculatum [17, 19, 20]. Therefore, the ability of A.italicum and A. maculatum to colonize new areas may account for their wider geographic range in comparison to diploids like A. pictum, or A. orientale [14]. However, the tetraploid A. apulum has a very limited distribution in Southern Italy [21] compared with the diploid A. alpinum has a very wide distribution [22].

Despite the genus being relatively well studied in Europe, there is no previous report on the karyotype structure of *A. cyrenaicum.* Therefore, the present study aims to provide the first karyotype analysis of *A. cyrenaicum* from Al-Jabal Al-Akhdar, Libya, including chromosome number, size, morphology, ploidy level, and the occurrence of satellites, which will contribute to cytogenetic characterization and support future taxonomic and evolutionary studies.

 ISSN: Online 2790-1637, Print 2790-1629
National Library of Libya, Legal number: 154/2018

Figure (1) *Arum cyrenaicum* Hruby in its natural habitat. (A)Habit of the plant, showing the sagittate leaves and long petioles.(B) Close-up of the dark purple, sail-shaped inflorescence consisting of the spathe and spadix.

2.MATERIALS and METHODS

2.1.Plant Material:

Plant samples of A. cyrenaicum Hruby were collected from natural habitats in the Tolmitha site, located in the Al-Jabal Al-Akhdar region, Cyrenaica, northeastern Libya, during 2021–2022. The site is characterized by reddish clay soil and a Mediterranean climate.

2.2.Experimental Method:

The seeds (isolated from the fruits) were germinated in petri dishes at 15°C for two weeks. Actively growing root tips were pretreated in 0.1% colchicine solution for 6 hours to arrest cells at metaphase. After pretreatment, the root tips were fixed in Carnoy's solution (glacial acetic acid: 95% ethanol, 1:3) for 24 hours at 4°C and subsequently stored in 70% ethanol at 4°C until further use. For slide preparation, fixed roots were hydrolyzed in 1 N HCl at 60°C for 20 minutes, rinsed in distilled water for 20 minutes, and then stained in 1% aceto-orcein solution (1 g orcein dissolved in 100 mL glacial acetic acid). Squash preparations were made by gently pressing the root tips under a coverslip for microscopic observation. At least ten metaphase cells were used to determine chromosome numbers and karyological characteristics. Photomicrographs were taken with a microscope at 1000 x magnification. 2.3karyotype Analysis:

Detected metaphase plates were recorded by computer; after that karyotypes were performed by cutting and arranging chromosomes with homologous pairs based on arm ratio and chromosome size using the ImageJ program[23] and Adobe Photoshop 2020 program.

The chromosome type was determined using the centromere position and arm ratio and classified according to Levan et al.[24]. The degree of karyotype asymmetry was estimated with Stebbins's method [25]. The following chromosomal measurements were recorded: chromosome length (CL), arm ratio (AR = L/S), Index of relative length of chromosome (IRL%= (CL/ΣCL) ×100), centromere index (CI%= S/CL ×100). Also, the following karyotype parameters were documented: degree of karyotype asymmetry (A=Mean (L − S) / (L + S) [26], intrachromosomal asymmetry (A_1=1-Mean S / L), interchromosomal asymmetry ($A_{2=}$ sCL/xCL [27], coefficient of variation of chromosome length (CVcL= A2×100)(), coefficient of variation of centromere index (CVcI = (sCI / x CI) × 100[28], Arano index (Ask%= (ΣL/ΣCL) ×100) [29], symmetry index S% = (CLmin/ CLmax)×100) [26], total form percen-tage of homologous chromosome pairs TF%= (ΣS/ΣCL) ×100 [30] and Asym-metry index (AI= (CVcL×CVci)/100) [28].

The Ideogram was drawn automatically by the Ideokar program, and the mean and standard deviations were analyzed for all chromosomal and karyotype parameters using the SPSS (version 13.0) statistical program.

3.RESULTS

All ten individuals/plants studied were identified as tetraploid 2n = 4x = 56 (Fig. 2), with a basic chromosome number of x = 14 and the ideogram is shown in (Figure.3). The karyotype analysis of this species revealed the existence of three distinct types of chromosomes, with the metacentric (M-m) type being more frequent than the submetacentric (sm) and subtelocentric (st) types (Table1). The karyotype formula (KF) includes 22 M-m pairs, 5 sm pairs, and 1 st pair. The formula was 6M + 38m + 10sm + 2st (2SAT). This is the first study to document the karyotype of A. cyrenaicum, which is considered an endemic species of Al-Jabal Al-Akhdar.

The analysis of 28 chromosomes from A. cyrenaicum revealed significant variation in the arm lengths and their ratios. The average length of the short arm (S) was 1.62 µm, while the average length of the long arm (L) was 2.20 µm, resulting in an average total chromosome length of 3.82 µm. The S/L ratio, which indicates the degree of symmetry between the two arms, ranged from 0.28 (chromosome 18) to 1.000 (chromosome 2), with an overall average of 0.74. Further analysis using the (L-S)/(L + S) index, which reflects the relative difference be-

 ISSN: Online 2790-1637, Print 2790-1629
National Library of Libya, Legal number: 154/2018

tween arm lengths, revealed a mean value of 0.15, reinforcing the presence of moderate arm length asymmetry in most chromosomes. The (L-S)/L index also averaged 0.24, which similarly supports this observation. Out of the 28 chromosomes, three chromosomes (2, 4, and 10) showed perfect symmetry (S ≈ L), classifying them as metacentric(M). In contrast, several chromosomes, such as 3, 7, 18, 23, 25, and 26, had noticeably low S/L ratios (below 0.65), indicating submetacentric to telocentric configurations. Chromosome 18 was identified as the most asymmetrical, with an S/L ratio of 0.28 and a (L-S)/(L + S) value of 0.56 (Table 1). The relative length of the chromosomes, indicated by the index of IRL%, ranged from 2.53% to 4.29%. The CI% ranged from 21.94% to 50.00%, with an average centromere position of 43.68%. The AR ranged from 1.00 to 3.55, with an average AR of 1.42 (Table 1).

The karyotype of this species is classified as a symmetry type 1A according to Stebbins classification. The average value of the A_1 and the average value of the A_2 for A. cyrenaicum are 0.26 and 0.19, respectively. The value of the CVcL = 19.31 and the value of the CVcI = 5.82.

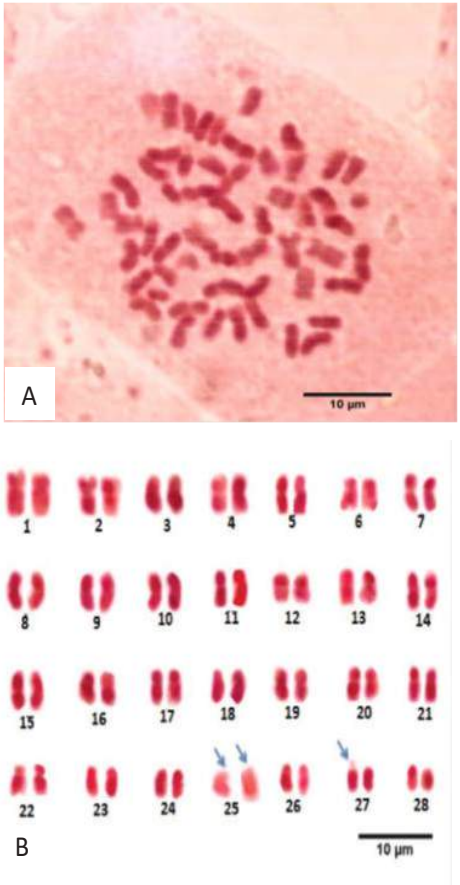

Figure 2. Metaphase chromosomes spread (A), and karyogram of *A. cyrenaicum*(B). Bar = 10 µm.

The values of the AI = 1.12, Ask% = 57.46, and the degree of A = 0.15, the values of the total S% = 61.01, and the total form percentage of TF% = 42.31 (Table 2) .

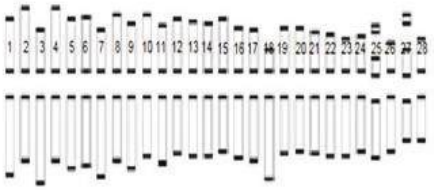

Figure 3. Idiograms of *A. cyrenaicum* based on chromosome length and primary and secondary constrictions (Satellites shaded on the short arms of pairs 25 and 27). Bar = 10 µm.

 ISSN: Online 2790-1637, Print 2790-1629
National Library of Libya, Legal number: 154/2018

5.DISCUSSION

5.1.Chromosome Number and Morphology:

Determining chromosome numbers has been a very useful approach for researchers to study evolutionary relationships and assess the impact of inbreeding depression [31]. Arum has a basic number of x=14, and three ploidy levels have been reported: diploid, tetraploid, and hexaploid. A. orientale, A. alpinum, A. hygrophilum, and A. pictum are diploid (2n=28), A. maculatum and A. apulum are tetraploid (2n = 56), while A. italicum is hexaploid (2n=84) [15,16, 21 ,32]. The tetraploid (2n = 4x = 56) observed here in A. cyrenaicum is consistent with Boyce's [33] findings but differs from that of Marchant [34], who reported a somatic chromosome number of 2n=28. This difference in chromosomal number could be due to the difficulty of counting or the small number of individuals studied. In the aforementioned works, only chromosome numbers have been reported. *A. cyrenaicum* (2n = 56) shares its chromosome number with A. apulum (supporting its placement in subsection Dischroochiton; Boyce[33]) and A. maculatum. However, *A. cyre-naicum* differs from both species in terms of its unique karyological features (e.g., high ratio of metacentric chromosomes and distinct chromosome size and morphology) may represent a unique adaption to its local environment in Libya. Additionally, its chromosome number and morphology are inconsistent with A. hygrophilum, A. pictum and A. italicum. Polyploidy is a common phenomenon in plants that occurs naturally and spontaneously. It results in the increase in genome size caused by the presence of three or more chromosome sets. Polyploidy is an important mechanism regarding speciation and evolution of plants, that occurs in two ways: autopolyploidy with genome dupli-cation in only one species and allopolyploidy with genome dupli-cation between species. D'Emerico et al. [16]; Bianco et al. [21]; and Turco et al. [15] state that the tetraploid Arum's chromosomes can be arranged in sets of two, and since it is impossible to arrange them in a series of four, it can be assumed that it is likely allopolyploid.

Table 1. Karyomorphometric measurements of *Arum cyrenaicum* (2n = 56, 4x) Short arm length (S), long arm length (L), total chromosome length (CL = S+L), arm ratio (S/L), relative length (CL/ΣCL ×100), centromeric index (S/(S+L)×100), chromosome type according to Levan et al. (1964).

Chr. No	S (µm)	L (µm)	(S+L)	S/L	L/S	(L-S)/L	(L-S) /(L+S)	(CL/ ΣCL)*100	S/(S+L)* 100	Chr. Type
1	1.93±.05	2.79±.16	4.72±.21	0.69±.31	1.44±.04	0.3±.68	0.18±.52	4.40±.15	40.88±.15	m
2	2.27±.03	2.27±.03	4.54±.06	1.00±1.0	1.00±.00	0.00±0.00	0.00±.00	4.23±.01	50.00±.00	M
3	1.53±.04	2.99±.05	4.52±.09	0.51±.8	1.96±.02	0.48±.2	0.32±.11	4.21±.03	33.84±.23	sm
4	2.19±.02	2.25±.06	4.44±.08	0.97±.3	1.03±.01	0.01±.67	0.01±.5	4.04±.03	49.32±.35	M
5	1.91±.02	2.50±.05	4.41±.08	0.76±.4	1.31±.01	0.23±.6	0.13±.37	4.11±.02	43.31±.22	m
6	1.97±.06	2.41±.07	4.38±.13	0.81±.85	1.22±.00	0.18±.14	0.1±.07	4.08±.07	44.97±.03	m
7	1.53±.01	2.77±.02	4.30±.01	0.55±.5	1.81±.03	0.44±.5	0.28±1.00	4.01±.04	35.58±.42	sm
8	2.02±.02	2.23±.03	4.25±.01	0.9±.67	1.10±.01	0.09±.3	0.04±1.00	3.96±.04	47.52±.55	m
9	1.73±.02	2.46±.05	4.19±.03	0.7±.4	1.42±.01	0.29±.6	0.17±1.00	3.91±.07	41.28±.25	m
10	2.01±.01	2.08±.02	4.09±.03	0.96±.5	1.03±.00	0.03±.5	0.01±.3	3.81±.00	49.14±.06	M
11	1.64±.00	2.37±.07	4.01±.06	0.69±.00	1.44±.04	0.3±1.00	0.18±1.16	3.74±.02	40.92±.73	m
12	1.91±.02	2.02±.02	3.93±.01	0.94±1.0	1.05±.03	0.05±.00	0.02±.00	3.66±.04	48.60±.59	m
13	1.83±.01	2.08±.01	3.91±.03	0.87±1.0	1.13±.00	0.12±.00	0.06±.00	3.64±.02	46.80±.06	m
14	1.71±.05	2.16±.07	3.87±.02	0.79±.71	1.26±.08	0.2±.28	0.11±1.00	3.61±.02	44.18±1.56	m
15	1.87±.04	1.97±.05	3.84±.02	0.94±.8	1.05±.05	0.05±.2	0.02±.5	3.58±.09	48.69±1.17	m
16	1.58±.03	2.19±.03	3.77±.01	0.72±1.0	1.38±.05	0.27±.00	0.16±.00	3.52±.05	41.90±.87	m
17	1.55±.06	2.17±.06	3.72±.01	0.71±1.00	1.40±.10	0.28±.00	0.17±.00	3.47±.1	41.67±1.74	m
18	0.79±.03	2.81±.03	3.60±.05	0.28±1.00	3.55±.08	0.71±.00	0.56±.00	3.35±.09	21.94±.41	st
19	1.52±.06	2.04±.06	3.56±.01	0.74±1.00	1.34±.10	0.25±.00	0.14±.00	3.32±.04	42.69±1.85	m
20	1.54±.03	1.99±.03	3.53±.01	0.77±1.00	1.29±.05	0.22±.00	0.12±.00	3.29±.04	43.62±1.00	m

Chr. No	S (µm)	L (µm)	(S+L)	S/L	L/S	(L-S)/L	(L-S) /(L+S)	(CL/ ΣCL)*100	S/(S+L)* 100	Chr. Type
21	1.51±.06	1.95±.11	3.46±.04	0.77±.54	1.30±.12	0.22±.45	0.12±1.25	3.23±.07	43.64±2.41	m
22	1.37±.02	2.04±.05	3.41±.02	0.67±.4	1.48±.06	0.32±.6	0.19±1.5	3.18±.05	40.17±0.97	m
23	1.24±.02	2.12±.02	3.36±.01	0.58±1.00	1.70±.03	0.41±.00	0.26±.00	3.13±.03	36.90±.46	sm
24	1.29±.01	1.97±.01	3.26±.02	0.65±1.00	1.52±.02	0.34±.00	0.2±.00	3.04±.01	39.57±.26	m
25	1.11±.05	2.04±.06	3.15±.12	0.54±.83	1.66±.12	0.45±.17	0.29±.08	2.93±.07	35.23±.39	sm
26	1.08±.02	2.01±.11	3.09±.14	0.53±.18	1.83±.06	0.46±.81	0.3±.64	2.88±.09	34.95±.77	sm
27	1.41±.03	1.61±.15	3.02±.18	0.87±.2	1.14±.08	0.12±.8	0.06±.67	2.82±.14	46.68±1.90	m
28	1.34±.02	1.54±.03	2.88±.04	0.87±.67	1.10±.00	0.12±.3	0.06±.25	2.68±.02	46.52±0.07	m
Average	1.62±.03	2.20±.05	3.82±.05	0.74±0.64	1.42±.04	0.24±.31	0.15±.42	3.56±.05	42.16±0.69	

Polyploids frequently have a wider geographical range than their diploid parents [35, 36], probably because they are preadapted to habitats and resources off limits to their parents [37]. They have a diversity of alleles that can confer a greater ecological niche than that of diploid progenitors [38]. Polyploidy associated with structural changes in chromosomes is involved in bringing about further diversification of karyotype morphology [25]. Therefore, on this basis, it is suggested that *A. cyrenaicum* is characterized by more rearrangement in its chromosome complement; these rearrangements may enhance the adaptive capacity of certain species. This exceptional tetraploid population of *A. cyrenaicum* could represent the starting point of evolutionary differentiation in this species. An average centromere position and arm ratio indicate a predominantly median position for the centromeres and predominantly metacentric chromosomes in the karyotype of A. cyrenaicum. The karyotype formula of this species consisted of 22 pairs metacentric, 5 pairs submetacentric, and 1 pair subtelocentric. Satellites were observed on the short arms of pairs 25 and 27 in *A .cyrenaicum*, the analyses show that the karyotype is similar to the previous reports for A. maculatum (26m+24sm+6st; microsatellite on the short arm of pair 27) and A. apulum (40m+16sm; secondary constriction on the short arm and a microsatellite on the long arm of pair 27 [15].

This is useful in characterizing a tetraploid Arum and studying the relationship between them. In general, the Araceae family presents metacentric, submetacentric, and sub-telocentric chromosomes [1]. In *A. cyrenaicum*, no B-chromosomes were observed during the study period.

Table 2. Karyomorphometric data for the studied plant taxa

Ch.size variation(µm)	THCL	CVci	Interchromosomal index		Intrachromosomal index				Symmetry Index S%	Asymmetry Index AI
			CVcI	A_2	TF%	AsK%	A	A1		
2.88-4.72	107.21±1.51	5.82±.45	13.55±.195	0.19±1.62	42.31±.56	56.131±.091	0.15 ±.39	0.26±.40	61.01±.19	1.12±.00

5.2 Chromosome Size

Chromosome length is useful for distinguishing individuals, samples, populations and species. It is also an indirect indicator of the total DNA content. Measurement of chromosome size correlates with evolutionary age, which provides an estimate of genome size using the chromosomal data [31,39].

Most species in the genus Arum possess small to medium-sized chromosomes, typically ranging from 2.65 to 5.40µm. In this study, the chromosome size of A. cyrenaicum (2.88-4.72µm) was comparable to that of A. alpinum (2.95-4.80µm) and A. maculatum(2.00-4.80µm) [16]. The THCL, a proxy for genome size [40,41], is calculated as the sum of the lengths of all the chromosomes in a metaphase plate, divided by the ploidy level [42]. The THCL of *A. cyrenaicum* (107.21µm) further confirms that this species has medium to small chromosomes.

5.3 Karyotype Asymmetry

Karyotype asymmetry is an important parameter in karyological studies [43]. It is further considered one of the most popular, inexpensive, and widely used approaches, especially by botanists. Karyotype symmetry has two components, one related to variation among chromosome size and the other to variation in centromere position [44].

This study revealed that most chromosomes in A. cyre-

 ISSN: Online 2790-1637, Print 2790-1629
National Library of Libya, Legal number: 154/2018

naicum are either metacentric or submetacentric. The karyotype symmetry indices exhibited low heterogeneity and variation values. The value of the intrachromosomal asymmetry index plays a role in finding variations in chromosome types within a karyotype. The range of values for the A_1 is from zero to one. The low value of (A_1) for A. cyrenaicum signifies a value close to zero and this, in turn, indicates a predominantly metacentric chromo-some in the karyotype of A. cyrenaicum. However, the value of the A_2 is used to assess the deviation (dispersion) in chromosome length within a karyotype [45]. The small value for A. cyrenaicum shows that the chromosomal length deviation in A. cyrenaicum is relatively small (Table 2). Furthermore, the value of the CVcL and the value of CVci indicates low variation in chromosome length and centromere index, respectively. According to Uysal et al. [46], the larger the values of and, the greater the asymmetry in the karyotype. Therefore, the low values of both and in A. cyrenaicum indicate that its karyotype is predominantly composed of symmetric chromosomes.

The karyotype of this species is classified as a symmetry type 1A according to Stebbins classification, indicating that the karyotype of A. cyrenaicum is symmetrical. The low values of the AI, Ask%, and degree of A indicate a relatively low level of asymmetry. Meanwhile, the high values of the total S%, total form percentage of TF%, and CI% indicate a symmetrical structure of the karyotype.

These findings demonstrate that A. cyrenaicum exhibits a distinct, symmetrical chromosomal pattern. Combined with morphological and geographical evidence, these cytological results support Hruby's [7] proposal that *A. cyrenaicum* warrants recognition as a distinct species. Although this species was recently recorded in 1992 in south-west Crete (Kakodikianos valley north of Paleohora as far as Kandanos), marking the first record of A. cyrenaicum outside Libya [47]. The analysis offered by the current study reveals that its symmetric karyotype is predominantly composed of meta-centric chromosomes closely resembling that of A. apulum. According to Stebbins [25], a high proportion of metacentric chromosomes may indicate early evolutionary divergence in a species.

REFERENCES

1.Saensouk, P.; Saensouk, S. and Senavongse, R. (2022) Cytogenetic studies of six species in the family Araceae from Thailand. Caryologia, 75(2): 5-13.

Jafri, S.M.H. and EL-Gadi, A.A. (1977) Flora of Libya: Araceae. Al-Faateh University, Tripoli, Libya, 41:1-9.

2.Abdulrraziq, A. A. and Salih, S. M. (2020) Morphological characterization of Arum cyrenaicum Hruby plant in Al-Jabal Al-Akhdar region-Libya. Al-Mukhtar Journal of Sciences, 35(3): 246-254

3.Al-Traboulsi, M. and Alaib, M. A. (2021) A Survey of medicinal plants of Wadi Al-Kouf in Al-Jabal Al-Akhdar, Libya. Natura Croatica: Periodicum Musei Historiae Naturalis Croatici, 30(2): 389-404.

4.El-Mokasabi, F. M. (2014) Floristic composition and traditional uses of plant species at Wadi Alkuf, Al-Jabal Al-Akhder, Libya. American Eurasian Journal Agriculture and Environment Sciences, 14(8): 685-697.

5.Abdel-karim, M.; Abdel-shafeek, A. K.; Saada, F. A. and Attafa, S. M. M. (2018) Isolation and characterization of some flavones from Arum cyrenaicum (Araceae). World Journal of Pharmaceutical and Life Sciences, 4(2): 27-33.

6.Hruby, J. (1912) Le genre Arum (The genus Arum). Bulletin de la Société Botaniqué de Geneve, 2(4):159.

7.Durand, E. and Barratte, G. (1910) Florae Libycae Prodromus (Prodrome of the Flora of Libya). Geneva.

Pampanini, R. (1931) Prodromo della Flora Cirenaica (Preliminary study of the Flora of Cyrenaica). Forli.(Abstract)

8.Sun, W.G.; Sun, H. and Li, Z.M. (2019) Chromosome data mining and its application in plant diversity research. Plant Science Journal, 37(2): 260-269.

9.Guerra, M. (2008) Chromo-some numbers in plant cytotaxonomy: Concepts and implications. Cytogenetic and Genome Research, 120(3-4):339-50.

10.Singh, R.; Kaur, R. and Tanisha, A. (2023) Chromo-some number of some medicinal angiosperms: A review article. International Journal of Botany Studies, 8(7):22-25.

11.Rivero, R.; Sessa, E.B. and Ferguson, R.Z. (2019) EyeChrom and CCDBcurator: Visualizing chromosome count data from plants. Applications in Plant Sciences, 7(1):1-5.

12.Prime, C. T. (1980) Arum L. In: Tutin, T.G.; Heywood, V.H.; Burges, N.A.; Moore, D. M.; Valentine, D.H.; Walters, S.M. and Webb, D.A.(eds.). Flora Europaea,5. Cambridge,(6): 269-271.

13.Turco, A.; Medagli, P.; Albano, A. and D'Emerico, S. (2014) Karyomorphometry on three polyploid species of

Arum L. (Araceae, Aroideae). Compa-rative Cytogenetics, 8(1):71-80.

14.D'Emerico, S.; Bianco, P. and Medagli, P. (1993) Chromosome numbers and karyotypes in Arum (Araceae). Caryologia, 46(2-3): 161-170.

15.Bedalov, M. (1981) Cyto-taxonomy of the genus Arum (Araceae) in the Balkan and Aegean area. Botanische Jahrbücher für Systematik, Pflanengeschichte und Pflanzengeographie, 102(1-4):183-200.

16.Bedalov, M. (1975a). Cyto-taxonomical and phyto-geographical investigation of the species A. italicum Miller in Jugoslavia. Acta Botanica Croatica, 34:143-50.

17.Meusel, H.; Jaeger, E. and Weinert, E. (1965) Verglei-chende chorologie der zentra-leuropäischen (Comp-arative chrology of the central European flora). Flora 1

18.Terpó, A. (1973) Kritische revision der Arum-Arten des karpatenbeckens (Critical revision of the Arum species of the Carpathian Basin). Acta Botanica Academiae Scienti-arum Hungaricae, 18: 216-255.

19.Bianco, P.; D'Emerico, S.; Medagli, P. and Bedalov, M. (1994) Indagini sistematiche su Arum apulum (Careno) Bedalov (Araceae), entita endemic delle Murge Pugliesi (Systematic investigations on Arum apulum (Carano) Bedalov (Araceae), endemic entity of Apulian Murge). Journal of Plant Taxonomy and Geography, 49(1):43-49.(Abstract)

20.Bedalov, M. and Fischer, M.A. (1995) Arum alpinum (Araceae) and its distribution in the Eastern Mediterranean. Phyton (Austria), 35(1): 103-113.

21.Schindelin J, Arganda-Carreras I, Frise E,(2012) Fiji: an open-source platform for biological-image analysis. Nature Methods. 9(7):676–682.

22.Levan, A.; Fredga, K. and Sandberg, A. A. (1964) Nomenclature for centromeric position on chromosomes. Hereditas, 52(2): 201-220.

23.Stebbins, G. L. (1971) Chromo-somal evolution in higher plants. Edward Arnold (Publishers) Ltd., London, UK.

24.Watanabe, K.; Yahara, T.; Denda, T. and Kosuge, K. (1999) Chromosomal evolution in the genus Brachyscome (Asteraceae): statistical tests regarding correlation between changes in karyotype and habit using phylogenetic information. Journal of Plant Research, 112(2): 145-161.

25.Romero-Zarco,C.(1986) A new method for estimating karyotype asymmetry. Taxon, 35(3):526-530.

Paszko, B. (2006) A critical review and a new proposal of karyotype asymmetry indices. Plant Systematics and Evolution, 258(1):39-48.

26.Arano, H. (1963) Cytological studies in subfamily Carduoideae (Compositae) of Japan IX. The karyotype analysis and phylogenic considerations on Pertya and Ainsliaea (2), Botanic Magazine, 76(895): 32-39.

27.Huziwara, Y. (1962) Karyotype analysis in some genera of Compositae VIII. Further studies on the chromosomes of Aster. American Journal of Botany, 49(2):116-119.

28.Contreras, R.N. and Ruter, J.M. (2011) Genome size estimates and chromosome numbers of Callicarpa L. (Lamiaceae). Horticultural Science, 46(4): 567-570.

29.Bedalov, M. and Drenkovski, R. (1997) The genus Arum (Araceae) in the F.Y.R. Makedonija. Bocconea, 5(2):781-785.

30.Boyce, P.C (1989) A new classification of Arum with keys to the infra generic taxa. Kew Bulletin, 44(3):383-395.

31.Marchant, C.J. (1973) Chromo-some variation in Araceae: V. Acoreae to Lasieae. Kew Bulletin, 28 (2): 199-210.

32.Schönswetter, P.; Lachmayer, M.; Lettner, C.; Prehsler, D.; Rechnitzer, S.; Reich, D. S. and Trávníček, P. (2007) Sympatric diploid and hexa-ploid cytotypes of Senecio carniolicus (Asteraceae) in the Eastern Alps are separated along an altitudinal gradient. Journal of Plant Research, 120(6):721-725.

33.Whittemore, A. T. and Olsen, R. T. (2011) Ulmus americana (Ulmaceae) is a polyploid complex. American Journal of Botany, 98(4): 754-760.

34.Levin, D. A. (2003) The ecological transition in speciation. New Phytologist, 161:91-96.

35.Pound, G. E.; Cox, S. J. and Doncaster, C. P (.2004) The accumulation of deleterious mutations within the frozen niche variation hypothesis. Journal of Evolutionary Biology, 17(3):651-662.

36.Mehra, P.N. and Bawa, K.S.1972. Cytogenetical evol-ution of hardwoods. Nucleus, 15: 64-83.

37.Carta, A. and Peruzzi, L. (2016) Testing the large genome constraint hypothesis: plant traits, habitat and climate seasonality in Liliaceae. New Phytologist, 210(2): 709-716.

38.Franzoni, J; Astuti, G; Bacchetta, G; Barone, G; Bar-

tolucci, F; Bernardo, L; Carta, A; Counti, F; Domina, G; Frajman, B; Giusso del Galdo, G; Iamonico, D; Iberite, M; Minuto, L; Sarigu, M; Terlevic, A; Turini, A; Varaldo, L; Volgger, D. and Peruzzi, L. (2024) A cytosystematic study of the Dianthus virgineus complex (Caryophyllaceae) in the Central Mediterranean. Journal of Systematics and Evolution, 62(4): 589-602.

39.Peruzzi, L. and Altinordu, F. (2014) A proposal for a multivariate quantitative appro-ach to infer karyological relationships among taxa. Comparative Cytogenetic, 8(4):337-349.

40.Eroğlu, H.E. (2015) Which chromosomes are subtelo-centric or acrocentric? A nem karyotype ymmetry/ asymmetry index. Caryologia, 68(3):239-245.

Peruzzi, L. and Eroğlu, H.E. (2013) Karyotype asymmetry: again, how to measure and what to measure?. Comparative Cytogenetics, 7(1): 1-9.

41.Muliawati,E.S; Hartati,S.; Parjanto,P.; Sukaya,S; Nandariyah,N.; Yuniastuti,E.; Manurung, I.R. and Purmiyoto, C.W.W. (2023) Karyotype of Phaius tankervilleae and Phaius amboinensis orchid. E3S Web Conferences, 373, 03029.

42.Uysal, T.; Tekkanat, B.S.; Sezer, E.N.S.; Ada, R. and Bozkurt, M. (2018) Karyotype analysis of some lines and varieties belonging to Carthamus tinctorius L. species. Anatolian Journal of Botany, 2(1):1-9.

43.Cretan Flora. (2025) Arum cyrenaicum. Cretan Flora. Published on the Internet; http://www.cretanflora.com/ 9 April 2025.

 ISSN: Online 2790-1637, Print 2790-1629
National Library of Libya, Legal number: 154/2018

Scientific Journal of University of Benghazi

SJUOB (2025) 38 (2) Applied Sciences: Tayeb. et . al, 103 – 113
www.sjuob.uob.edu.ly

Antibacterial Efficacy of Origanum majorana and Salvia officinalis Extracts Against Escherichia coli and Staphylococcus aureus

Ahmed. Y. Tayeb [1]*, Anas. Y. Tateb[1], Amany. Y. Tayeb [2]

1. Laboratory of Plant Department, Faculty of Science, University Benghazi, Marj, Libya.
2. Department of Laboratory, Higher Health Institute, Marj, Libya.

DOI: 10.37376/sjuob.v38i2 | Received:11/08/2025 | Accepted:28/11/2025 | Publishing: 23/12/2025

ABSTRACT

This study evaluated the antibacterial activity of aqueous, ethanol, and essential oil extracts of Origanum majorana and Salvia officinalis against two human pathogens Escherichia coli and Staphylococcus aureus and determined their minimum inhibitory concentrations MICs. The findings indicated that the essential oil extracts were more effective in inhibiting bacterial growth compared to the aqueous and ethanolic extracts. O. majorana essential oil produced the largest inhibition zones: 2.38 cm against Escherichia coli and 2.98 cm against Staphylococcus aureus. Salvia officinalis essential oil showed moderate activity, with inhibition zones of 1.45 cm against E. coli and 1.40 cm against S. aureus. The ethanolic extracts produced limited inhibition (for example, S. officinalis ethanolic extract: 0.57 cm against E. coli; S. officinalis ethanolic extract: 2.17 cm against S. aureus; O. majorana ethanolic extract: 0.45 cm against S. aureus. The aqueous extracts generally exhibited weak activity, except for the O. majorana aqueous extract against E. coli inhibition 2.20 cm and S. officinalis aqueous extract against S. aureus inhibition 1.15 cm. Compared with standard antibiotics tetracycline , chloramphenicol some essential-oil treatments especially marjoram showed comparable activity. The results showed that the essential oils exhibited the strongest antibacterial effect. Among them, O. majorana oil was the most active. Based on these observations, the essential oils of O. majorana and S. officinal might serve as promising natural antibacterial agents and could potentially be applied in combination with standard antibiotics.

KEYWORDS: Origanum majorana, Salvia officinalis, essential oils, aqueous extract, alcoholic extract, Escherichia coli, Staphylococcus aureus, antibacterial activity, and minimum inhibitory concentration.

Corresponding Author: Ahmed. Y. Tayeb, ahmed.tayeb@uob.edu.ly.

 ISSN: Online 2790-1637, Print 2790-1629
National Library of Libya, Legal number: 154/2018

1.INTRODUCTION

The use of plants as source of remedies for the treatment of many diseases dated back to prehistory and people of all continents have this old tradition. The search for agents to cure infectious diseases began long before people were aware of the existence of microbes. These early attempts used natural substances, usually native plants or their extracts and many of these herbal remedies proved successful (Sofowora, 1982). World Health Organization survey indicated that about 70-80% of the world's population rely on nonconventional medicine, mainly of herbal sources, in their primary healthcare. This is especially the case in developing countries where the cost of consulting a western style doctor and the price of medication are beyond the means of most people (Chan, 2000). Origanum majorana and Salvia officinalis, both members of the Lamiaceae family, are aromatic herbs traditionally used in cooking, folk medicine, and the pharmaceutical industry (Viuda-Martos et al., 2010; Hussain et al., 2010).

Their essential oils are particularly rich in monoterpenes such as thymol, carvacrol, and 1,8-cineole, which have been associated with strong antimicrobial and antioxidant activities (Burt, 2004; Teixeira et al., 2013).

The rapid emergence of antibiotic-resistant bacteria has become a major global health problem (Ventola, 2015; WHO, 2020). Consequently, identifying new and effective antibacterial agents from natural origins has become a priority. The present study focuses on the antibacterial potential of O. majorana and S. officinalis extracts specifically their aqueous, ethanolic, and essential oil forms against two clinically important bacterial species: E. coli and S. aureus.

The primary goal of this research was to compare the inhibitory effects and minimum inhibitory concentrations of the different extracts, and to determine which type of extract demonstrates the strongest antibacterial activity.

2.MATERIALS AND METHODS

2.1. Media preparation

a. Nutrient agar: Prepared according to the manufacturer's instructions (Condalab): 23 g per 1 L distilled water, sterilized at 121 °C for 15 minutes, stored until use.

b. Mueller–Hinton agar: Prepared by dissolving 38 g per 1 L distilled water and sterilized as above. Used for antibacterial testing.

2.2. Bacterial isolates included in the study

Pure bacterial isolates (mentioned in Table 1 below) which was obtained from your doctor's Laboratory in Almarj city.

Table (1): Bacterial isolates included in the study

Gram positive	Gram negative
Staphylococcus aureus	Escherichia coli

2.3 Plant material

Leaves of O. majorana and S. officinalis were purchased from local markets, Washed with tap water followed by distilled water, air-dried at room temperature, Ground to fine powder, and stored in sealed containers until extraction.

Table (2): Plant used in the study

User Part	Plant Family	The Scientific Name
Leaves	Lamiaceae	Origanum Majorana
Leaves	Lamiaceae	Salvia Officinalis

3.4 Preparation of plant extracts

Figure (1): Salvia officinalis

 ISSN: Online 2790-1637, Print 2790-1629
National Library of Libya, Legal number: 154/2018

Figure (2): Origanum Majorana

3.4.1. Preparation of aqueous extract:

The method (Ahmed et al., 1998) was used to prepare aqueous extracts by mixing 20 g of plant power for each plant sample separately with 400 ml of distilled water in a 1000ml volumetric flask, then leaving the suspension in a shaking water bath at a temperature of 40 c for a period. 24 hours, then suspension was filtered using several layers of medical gauze, then sterile glass bottle and placed in a flat glass dish in an electric oven at 40 degrees for 48 hours until the sediment from the filtrate became a powder stuck to the glass, then it was scraped off and collected in an airtight glass container. Close and store the extract after weighing in the refrigerator until use.

3.4.2. Preparation of alcoholic:

Use 96% ethanol alcohol as a solvent to prepare the alcoholic extract (Khanzada, 2006) for the plant sample using the same method used to prepare the aqueous extract

3.4.3. Preparation of volatile oil:

The volatile oil was extracted for each plant sample tested separately using the hydra distillation method according to the standard method (European pharmacopeia, 2008), where 100 grams of dry plant powder was weighed, 750 ml of distilled water was added to it, and it was placed in the distillation system for up to 4 hours, and the distillate was collected. (Volatile oil and water) were filtered through anhydrous sodium sulfate on filter paper no (1) the obtained volatile oil was weighed and stored in dark containers at -18 c.

3.5. Preparing different concentrations of plant extracts: aqueous, alcoholic, and volatile oils

Different concentrations of oils were prepared based on the method (Hadizadeh et al, 2009) by dissolving the required amount in a 0.05% Tween 20 solution to obtain concentrations ranging from…..ppm to….. ppm of the tested oil.

Likewise, the method for alcoholic extracts, or for aqueous extracts, is the same as the previous method, but instead of using tween, use distilled water for dissolution. Concentrations (300, 150, and 75) mg/ml were used for all extracts it is twofold dilution.

3.6. Antibacterial Activity and Determination of Minimum Inhibitory Concentration (MIC)

The antibacterial activity of the extracts was evaluated using the agar well diffusion method (Bloomfield, 1991). Muller–Hinton Agar was poured into sterile Petri dishes and inoculated with 100 µL of bacterial suspension evenly spread over the surface. Wells (8 mm in diameter) were made using a sterile cork borer.

Different concentrations of each extract (300, 150 and 75 mg/mL) were prepared:

Essential oils were dissolved in 0.05% Tween 20.

Ethanolic and aqueous extracts were dissolved in ethanol or distilled water, respectively.

A 100-µL aliquot of each concentration was placed into separate wells. Plates were left for 30 min at room temperature to allow diffusion and then incubated at 37 °C for 24 h. The diameter of inhibition zones was measured in millimeters. The lowest concentration that completely inhibited visible bacterial growth was recorded as the MIC.

3.7. Commercial antibiotics

To compare the effectiveness of plant extracts with some common commercial antibiotics two antibiotics were used; Tetracycline (10 ug) and Chloramphenicol (5 ug). The antibiotic disc was placed on the surface of the MHA solid medium in the petri dish, and then incubated for 24 hours at 37 c. After incubation, the inhibition zone around the disc was measured for

each plante and considered as a positive control.

3.RESULTS

3.1 Effect of volatile oils of tested plants against E.coli and comparison with tested antibiotics

The effect of the volatile oil of the tested plants against E.coli was explained in Table (3). Marjoram oil showed the strongest effect against E. coli, with an inhibition zone of 2.38 cm.

The minimum inhibitory concentration for both Salvia and marjoram oils was 75 mg/mL, while Salvia oil required a higher concentration of 300 mg/mL to inhibit E. coli growth.

Table (3): Effect of volatile oils of tested plants against E. col and comparison with tested antibiotics

E. coli				
Plant	300 mg/ml	150 mg/ml	75mg/ml	MIC (mg/ml)
	Inhibition Zone (cm)			
Marjoram	2.383 a	2.117	1.667	75
Salvia officinalis	1.450 d	0.000	0.000	300
Control	0.000 c	0.000	0.000	-
L.S.D	0.2717**			
Antibiotics	Inhibition Zone (cm)			
Chloramphenicol(5ug)	1.117			
Tetracycline(10ug)	3.267			
Control	0.000			

Means followed by different letters (a, b, c, d) within the same column are significantly different at $P \leq 0.05$ according to LSD test.

3.2. Effect of alcohol extracts of tested plants against E.coli and comparison with tested antibiotics

The results revealed that E.coli growth inhibited by only the ethanol extract of Salvia 0.5667 cm whereas no effects were reported for the rest of plants Table(4).

When the alcoholic extracts of plants were tested against E.coli with concentrations ranged from 75 to 300 mg/ml, only Salvia plant exhibited an inhibitory effect at a concentration of 300 mg/ml. Regarding the MIC of the alcoholic extract of Salvia value of 300mg/ml.

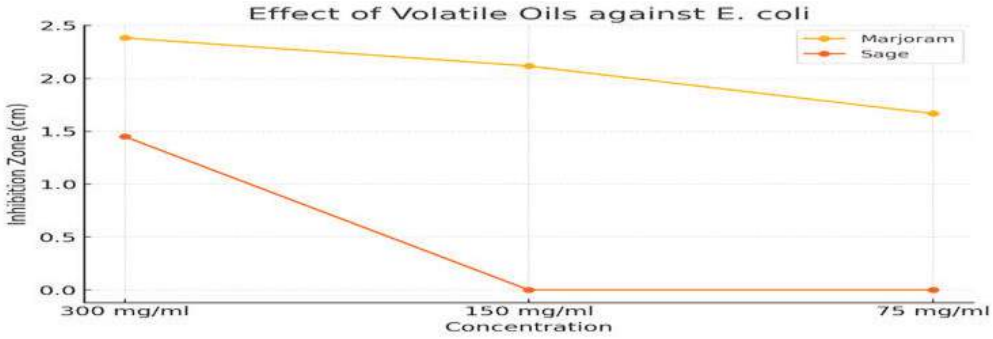

Figure (3): Effect of Origanum majorana and Salvia officinalis essential oils on E. coli at different concentrations

 ISSN: Online 2790-1637, Print 2790-1629
National Library of Libya, Legal number: 154/2018

Table (4): Effect of alcoholic extracts of tested plants against E. coli and comparison with tested antibiotics

Escherichia coli				
Plant	300 mg/ml	150 mg/ml	75mg/ml	MIC (mg/ml)
	Inhibition Zone (cm)			
Marjoram	0.000	0.000	0.000	-
Salvia officinalis	0.5667	0.000	0.000	300
Control	0.000	0.000	0.000	-
L.S.D	0.05418**			
Antibiotics	Inhibition Zone (cm)			
Chloramphenicol(5ug)	3.267			
Tetracycline (10ug)	1.117			
Control	0.000			

Means followed by different letters (a, b, c, d) within the same column are significantly different at $P \leq 0.05$ according to LSD test.

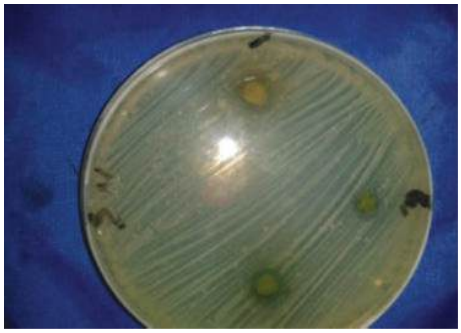

Figure (4): The alcoholic extract of O. majorana showed no inhibitory activity against E. coli at all tested concentrations (75–300 mg/mL).

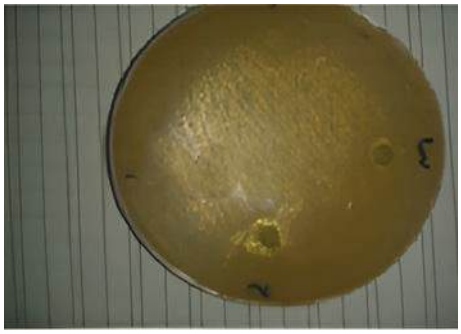

Figure (5): The alcoholic extract of S. officinalis exhibited limited antibacterial activity, with an inhibition zone of 0.56 cm at 300 mg/mL only.

3.3. Effect of aqueous extracts of tested plants against E.coli and comparison with tested antibiotics

The aqueous extracts of the tested plants were generally less active against E. coli, as shown in Table (5). With exception of marjoram aqueous extract at the concentration of 300 mg/ml, which exhibited an inhibitory zone of 2.200 cm.

And the MIC at the same concentration, the rest of plants showed no effect on E.coli at all concentrations used.

As for the minimum inhibitory concentration (MIC) for the extract against E.coli, the lowest inhibitory concentration for the marjoram plant was 300mg/ml.

 ISSN: Online 2790-1637, Print 2790-1629
National Library of Libya, Legal number: 154/2018

Table (5): Effect of aqueous extracts of tested plants against E.coli and comparison with tested antibiotics

E.coli				
Plant	300 mg/ml	150 mg/ml	75mg/ml	MIC (mg/ml)
	Inhibition Zone (cm)			
Marjoram	2.200 b	0.000	0.000	300
Salvia officinalis	0.000 a	0.000	0.000	-
Control	0.000 a	0.000	0.000	-
L.S.D	0.07762**			
Antibiotics	Inhibition Zone (cm)			
Chloramphenicol(5ug)	3.267			
Tetracycline (10ug)	1.117			
Control	0.000			

Means followed by different letters (a, b, c, d) within the same column are significantly different at $P \leq 0.05$ according to LSD test.

3.4. Effect of plant extracts used against S.aureus and comparison with tested antibiotic

Effect of volatile oils of tested plants against S.aureus and comparison with tested antibiotics Table (6) shows the results of the volatile oils of the tested plants against S. aureus, again the marjoram oil highest inhibitory effect, as the inhibition zone reached a value of 2.983cm, Whereas the least effect was reported for the Salvia extract (1.400cm).

The results showed significant differences between the tested plants in their effects on S. aureus at the 0.05 significance level. Where concentrations ranged from 75 to 300 mg/ml, the MIC test showed that S.aureus was more sensitive to all concentration except to sage as a higher MIC of 150 mg/ml was recorded in comparison 75 mg/ml for the rest.

Table (6): Effect of volatile oils of tested plants against S.aureus and comparison with tested antibiotics

S. aureus				
Plant	300 mg/ml	150 mg/ml	75mg/ml	MIC (mg/ml)
	Inhibition Zone (cm)			
Marjoram	2.983 a	2.400	2.300	75
Salvia officinalis	1.400 d	0.550	0.000	150
Control	0.000 e	0.000	0.000	
L.S.D	0.6571**			
Antibiotics	Inhibition Zone (cm)			
Chloramphenicol(5ug)	2.683			
Tetracycline(10ug)	2.550			
Control	0.000			

Means followed by different letters (a, b, c, d) within the same column are significantly different at $P \leq 0.05$ according to LSD test.

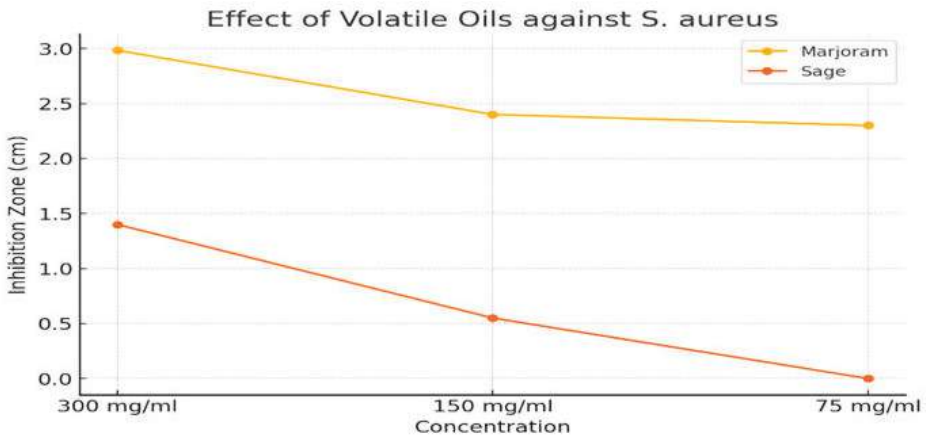

Figure (6): Effect of Origanum majorana and Salvia officinalis essential oils on S. aureus at different concentrations.

3.5. Effect of alcohol extracts of tested plants against S.aureus and comparison with tested antibiotics

Table (7) shows the results of the effect of plant extracts on S.aureus it was clear that salvia were the most effective and showed the same effect, as the inhibition zone reached a value of 2.167, then marjoram extract with the least inhibitory effect (0.450cm). MICs results against S.aureus, are illustrated in the same table, where all extracts showed the same MIC values of 150mg/ml

Table (7): Effect of alcohol extracts of tested plants against S.aureus and comparison with tested antibiotics

S.aureus				
Plant	300 mg/ml	150 mg/ml	75mg/ml	MIC (mg/ml)
	Inhibition Zone (cm)			
Marjoram	0.450 a	0.300	0.000	150
Salvia officinalis	2.167 c	1.817	0.000	150
Control	0.000 d	0.000	0.000	-
L.S.D	0.1417**			
Antibiotic	Inhibition Zone (cm)			
Chloramphenicol(5ug)	2.683			
Tetracycline(10ug)	2.550			
Control	0.000			

Means followed by different letters (a, b, c, d) within the same column are significantly different at $P \leq 0.05$ according to LSD test.

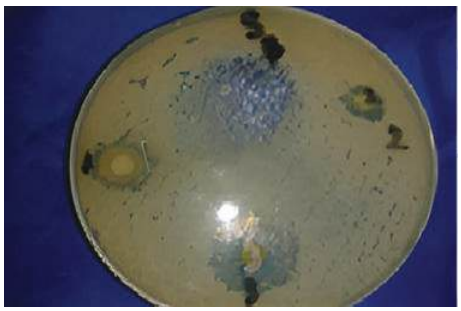

Figure (7): The alcoholic extract of O. majorana displayed weak antibacterial activity against S. aureus, with a maximum inhibition zone of 0.45 cm at 300 mg/mL

Figure (8): The alcoholic extract of S. officinalis demonstrated relatively strong antibacterial activity against S. aureus, producing inhibition zones up to 2.17 cm at 300 mg/mL.

3.6. Effect of aqueous extracts of tested plants against S.aureus and comparison with tested antibiotics

Table (8) shows the results of the effect of the aqueous extracts of the tested plants against S.aureus. Salvia extracted more effect against this bacterium as the inhibitory zone reached a value of 1.150cm.

While the marjoram extracts showed no effect against S.aureus at all concentrations. The Salvia extract exhibited an effect at two concentrations, 300mg/ml and 150mg/ml, and showed no effect at a concentration of 75mg/ml. As for the marjoram extracts, they showed no effect at all concentrations.

Table (8): Effect of aqueous extracts of tested plants against s.aureus and comparison with tested antibiotics

S.aureus				
Plant	300 mg/ml	150 mg/ml	75mg/ml	MIC (mg/ml)
	Inhibition Zone (cm)			
Marjoram	0.000	0.000	0.000	-
Salvia officinalis	1.150	0.917	0.000	300
Control	0.000	0.000	0.000	-
L.S.D	0.1390**			
Antibiotics	Inhibition Zone (cm)			
Chloramphenicol(5ug)	2.683			
Tetracycline(10ug)	2.550			
Control	0.000			

Means followed by different letters (a, b, c, d) within the same column are significantly different at $P \leq 0.05$ according to LSD test.

Table (9): Effect of commonly used commercial antibiotics against tested bacteria.

S.A*	L.M*	E.C*	S.T*	Antibiotics
2.550	2.500	1.117	0.967	Tetracycline
2.683	3.250	3.267	2.967	Chloramphenicol
0.5062***	L.S.D			

Means followed by different letters (a, b, c, d) within the same column are significantly different at $P \leq 0.05$ according to LSD test.

Table (10): Comparison of the effect of Salvia officinalis plant extracts with antibiotics against tested bacteria.

Tetracycline	Chloramphenicol	Aqueous	Alcoholic	Volatile oils	Bacteria
1.117	3.267	0.000	0.000	2.056	E.coli
2.550	2.683	0.611	0.250	2.561	S. aureus

Means followed by different letters (a, b, c, d) within the same column are significantly different at $P \leq 0.05$ according to LSD test.

Table (11): Comparison of the effect of Marjoram plant extracts with antibiotics against tested bacteria.

Tetracycline	Chloramphenicol	Aqueous	Alcoholic	Volatile oils	Bacteria
1.117	3.267	0.733	0.000	1.194	E.coli
2.550	2.683	0.000	0.700	1.372	S.aureus

Means followed by different letters (a, b, c, d) within the same column are significantly different at $P \leq 0.05$ according to LSD test.

4.DISUSSION

The results of this study showed clear differences in the antibacterial effects of the plant extracts tested. Overall, the essential oils demonstrated stronger inhibitory activity than both the alcoholic and aqueous extracts. This agrees with the findings of (Abdalla and Abdelgadir 2016).

The essential oil and aqueous extract of majorana in particular showed clear inhibition of bacterial growth, similar to what was reported by (Busatta et al. 2008). The weak antibacterial activity of the ethanolic and aqueous extracts may be due to the low levels of volatile compounds or the absence of important hydrophobic molecules that are usually concentrated in essential oils. Water, in particular, was not an effective solvent for extracting such compounds, which may explain the limited inhibitory activity observed (Merillon & Riviere, 2018).

When compared with the commercial antibiotics used in this study tetracycline and chloramphenicol the essential oils, especially which of O. majorana, showed similar or slightly lower inhibition. This suggested that these oils had real antibacterial potential, but cannot fully replace conventional antibiotics.

Unlike antibiotics, which act through defined biochemical mechanisms (for example, tetracycline inhibits protein synthesis), essential oils usually act through broader mechanisms such as damaging the bacterial membrane, denaturing proteins, and inducing oxidative stress (Burt, 2004).

The antibacterial activity of essential oils is likely related to multiple simultaneous effects on bacterial cells. Because of this multi-target action, bacteria may find it more difficult to develop resistance compared to when exposed to a single-mechanism synthetic antibiotic. (Merillon & Riviere, 2018).

Therefore, the findings of this study indicate that plant extracts, particularly the essential oils, may be useful as supportive antimicrobial agents. However, they should not be considered a substitute for conventional antibiotics, but rather a possible addition to current treatment approaches.

The higher antibacterial activity of O. majorana essential oil compared to S. officinalis

 ISSN: Online 2790-1637, Print 2790-1629
National Library of Libya, Legal number: 154/2018

may be related to its chemical composition. Marjoram oil contains higher amounts of phenolic monoterpenes such as thymol, carvacrol, and terpinen-4-ol, which are known for their strong antibacterial properties (Lambert et al., 2001; Burt, 2004).

By contrast, S. officinalis essential oil has more 1,8-cineole and camphor, which are less potent antibacterial agents, explaining its lower inhibitory zones. Overall, the findings support earlier studies that highlighted the potential of O. majorana and S. officinalis essential oils as natural antimicrobial agents (Burt, 2004; Özcan & Erkmen, 2001; Teixeira et al., 2013).

These results reinforce the importance of continued research on essential oils as promising natural products to combat bacterial infections, especially in light of the growing problem of antibiotic resistance worldwide.

5. CONCLUSION

This study demonstrated that O.majorana and S.officinalis possess noticeable antibacterial activity, especially in their essential oil forms. The essential oils showed much stronger inhibition of bacterial growth than the ethanolic and aqueous extracts. Among all treatments, the essential oil of O. majorana was the most active, producing inhibition zones of 2.38 cm against E. coli and 2.98 cm against S. aureus, with a minimum inhibitory concentration of 75 mg/mL. In comparison, S. officinalis essential oil showed moderate antibacterial action, with inhibition zones of 1.45 cm for E. coli and 1.40 cm for S. aureus, and higher MIC values (300 mg/mL and 150 mg/mL, respectively).

The ethanolic and aqueous extracts were generally weak in their antibacterial effects, suggesting that volatile components such as thymol, carvacrol, and 1,8-cineole are mainly responsible for the strong antibacterial properties observed in the essential oils.

The findings also showed that S. aureus was more sensitive to the essential oils than E. coli, which may be related to differences in the structural composition of their cell walls. Although the essential oils did not exceed the activity of the commercial antibiotics used for comparison, the inhibition zones produced by O. majorana oil were sufficiently notable to suggest possible practical applications.

Further work is needed to identify the specific bioactive compounds responsible for the antibacterial activity and to evaluate the safety and effectiveness of these oils in vivo. Investigating their combined use with existing antibiotics may also help determine whether they can enhance antibacterial efficacy or reduce required antibiotic dosages.

REFERENCES

1.Ahmed, M., Salam, A., & Younis, M. (1998). Antimicrobial activity of some medicinal plant extracts against bacteria and fungi. Pakistan Journal of Biological Sciences, 1(1), 45–50.

2.Abdalla, M. A., & Abdelgadir, H. A. (2016). Antibacterial activity of some medicinal plant extracts against pathogenic bacteria. Journal of Medicinal Plants Research, 10(5), 45–51.

3.Bloomfield, S. F. (1991). Methods for assessing antimicrobial activity. In S. F. Bloomfield, C. A. Morris, C. Looney, & R. G. Baird (Eds.), Methods for assessing antimicrobial activity (pp. 1–22). Blackwell Scientific Publications.

4.Busatta, C., Vidal, R. S., Popiolski, A. S., Mossi, A. J., Dariva, C., Rodrigues, M. R. A., Corazza, F. C., Corazza, M. L., Vladimir Oliveira, J., & Cansian, R. L. (2008). Application of Origanum majorana L. essential oil as an antimicrobial agent in sausage. Food Microbiology, 25(1), 207–211.

5.Burt, S. (2004). Essential oils: Their antibacterial properties and potential applications in foods—a review. International Journal of Food Microbiology, 94(3), 223–253.

6.Chouhan, S., Sharma, K., & Guleria, S. (2017). Antimicrobial activity of some essential oils—Present status and future perspectives. Medicinal

Chemistry, 7(3), 1–13. https://doi.org/10.4172/2161-0444.1000476.

7.Cushnie, T. P. T., & Lamb, A. J. (2011). Recent advances in understanding the antibacterial properties of flavonoids. International Journal of Antimicrobial Agents, 38(2), 99–107.

8.European Pharmacopoeia. (2008). European Pharmacopoeia (6th Ed.). Council of Europe.

9.Hadizadeh, I., Peivastegan, B., & Kolahi, M. (2009). Antifungal activity of essential oils from some medicinal plants of Iran against Alternaria alternata. American-Eurasian Journal of Agricultural & Environmental Sciences, 5(2), 305–309.

10.Hussain, A. I., Anwar, F., Nigam, P. S., Ashraf, M., & Gilani, A. H. (2010). Seasonal variation in content, chemical composition and antimicrobial and cytotoxic activities of essential oils from four Origanum species. Journal of the Science of Food and Agriculture, 90(11), 1827–1836.

11.Khanzada, S. K. (2006). Chemical constituents and antibacterial activity of Glycyrrhiza glabra Linn. Journal of Ethnopharmacology, 91(2–3), 381–385. https://doi.org/10.1016/j.jep.2004.09.015

12.Lambert, R. J. W., Skandamis, P. N., Coote, P. J., & Nychas, G.-J. E. (2001). A study of the minimum inhibitory concentration and mode of action of oregano essential oil, thymol and carvacrol. Journal of Applied Microbiology, 91(3), 453–462

13.Merillon, J. M., & Riviere, C. (Eds.). (2018). Natural antimicrobial agents. Springer International Publishing. https://doi.org/10.1007/978-3-319-67045-4

14.Özcan, M., & Erkmen, O. (2001). Antimicrobial activity of the essential oils of Turkish plant spices. European Food Research and Technology, 212(6), 658–660.

15.Owolabi, M. S., Ogundajo, A., Yusuf, K. O., Lajide, L., Villanueva, H. E., Tuten, J. A., Setzer, W. N., & Ogundajo, A. L. (2007). Chemical composition and bioactivity of the essential oil of Lantana camara L. from Nigeria. Records of Natural Products, 1(3), 128–134.

16.Teixeira, B., Marques, A., Ramos, C., Serrano, C., Matos, O., Neng, N. R., Nogueira, J. M. F., Saraiva, J. A., & Nunes, M. L. (2013). Chemical composition and antibacterial and antioxidant properties of commercial essential oils. Industrial Crops and Products, 43, 587–595.

17.Uniyal, S. K., Singh, K. N., Jamwal, P., & Lal, B. (2006). Traditional use of medicinal plants among the tribal communities of Chhota Bhangal, Western Himalaya. Journal of Ethnobiology and Ethnomedicine, 2(1), 1–14. https://doi.org/10.1186/1746-4269-2-14

18.Ventola, C. L. (2015). The antibiotic resistance crisis: Part 1: Causes and threats. Pharmacy and Therapeutics, 40(4), 277–283.

19.Viuda-Martos, M., Ruiz-Navajas, Y., Fernández-López, J., & Pérez-Álvarez, J. A. (2010). Spices as functional foods: A review. Critical Reviews in Food Science and Nutrition, 51(1), 13–28.

20.World Health Organization. (2020). Antibacterial agents in clinical development: An analysis of the antibacterial clinical development pipeline.

 ISSN: Online 2790-1637, Print 2790-1629
National Library of Libya, Legal number: 154/2018

Medical Sciences

Scientific Journal of University of Benghazi

SJUOB (2025) 38 (2) Medical Sciences: Abdallah & Abu Awaja, 115 – 125
www.sjuob.uob.edu.ly

Development and Quality Evaluation of Immune-Boosting Jelly Candy Using Natural Ingredients.

Hagir Mohamedsalih Abdallah [1]*, Alaa Attia Amer Abu Awaja [1].

1.Department of Health Nutrition/ Faculty of Public Health- Aljemail/ Sabratha University/ Sabratha/ Libya.

DOI: 10.37376/sjuob.v38i2 | Received:02/09/2025 | Accepted:28/11/2025 | Publishing: 23/12/2025

ABSTRACT

This study aimed to develop jelly candy with natural ingredients that have immune-boosting properties. Four candy samples were prepared from ingredients including lemon, beetroot, carrot, orange, pomegranate, strawberry, ginger, turmeric, black pepper, and gelatin. Two samples were sweetened with natural honey, and two with stevia sugar. Traditional gelatin candy from the local market was used for comparison. The samples were subjected to analysis of chemical quality properties, proximate composition, phytochemical analysis, mineral content, microbial analysis, and sensory evaluation. The most important results obtained showed that the prepared samples contained good levels of protein, fiber, and potassium, which were 6.87±0.009%, 3.55±0.003%, and 64±2 ppm, respectively. The beetroot, pomegranate, and strawberry samples had excellent iron content (35±2 and 31±2 ppm) for the honey-sweetened and stevia-sweetened samples, respectively. The preliminary screening results for phytochemical compounds showed that the prepared samples were rich in phenols, glycosides, and tannins (+++), while the samples sweetened with natural honey had excellent saponin content (+++). Microbial analysis revealed that the samples were free of coliform bacteria and E. coli. Sensory evaluation results revealed that the participants preferred the stevia-sweetened samples in all tested attributes, including color, taste, flavor, and overall acceptability, with a (very good) rating. The study recommended the development of a functional food industry based on natural food ingredients rich in macro- and micronutrients and active chemical compounds.

KEYWORDS: jelly candy, immunity booster, functional food, phytochemical compounds, coliform bacteria..

Corresponding Author: Hagir M. Abdallah, drhajarsalih@gmail.com.

 ISSN: Online 2790-1637, Print 2790-1629
National Library of Libya, Legal number: 154/2018

1.INTRODUCTION

The confectionery industry is one of the largest global food sectors; however, traditional jelly candies remain nutritionally poor due to their formulation, which typically relies on high amounts of sucrose and glucose, combined with gelling agents such as gelatin, starch, and corn syrup, as well as organic acids, colorings, and flavorings. Such compositions provide minimal nutritional value and may contribute to several health concerns, including dental caries, increased cravings, elevated blood glucose levels, and a higher risk of developing type 2 diabetes (Amer and Abd El-Rahman, 2023; Marfil et al., 2012; Burey et al., 2009; Tarahi et al., 2024). These limitations have raised awareness of the need to reformulate confectionery products into healthier alternatives.

In response, the concept of functional foods has gained considerable interest. Functional foods are designed to offer health benefits beyond basic nutrition by supplying essential macro- and micronutrients, antioxidants, and bioactive compounds that play vital roles in supporting immunity, reducing inflammation, and enhancing overall well-being (Singh et al., 2023; Abdallah et al., 2023). The increased demand for natural, health-promoting foods has encouraged the use of fruits and vegetables as alternative ingredients in food product development due to their richness in vitamins, minerals, polyphenols, and fiber (Devirgiliis et al., 2024).

In addition, herbs and natural plant extracts have emerged as promising contributors to functional food innovations because they contain diverse bioactive constituents—such as terpenoids, flavonoids, and beta-glucans—known for their immunomodulatory and protective effects. Probiotics, prebiotics, and plant-derived melatonin have also demonstrated potential in reducing inflammation and improving gut and immune health (Gasmi et al., 2023). Likewise, natural sweeteners and fruits such as pomegranate, citrus, and ginger provide valuable antioxidants and micronutrients that support cardiovascular, metabolic, and cognitive health (Vishwaarma et al., 2022; Stephen et al., 2023). Taken together, incorporating fruits, vegetables, herbs, and natural sweeteners into confectionery products represents a practical strategy to enhance their functional value while meeting the growing consumer demand for healthier and more natural alternatives. Therefore, this study aimed to develop an innovative functional jelly candy enriched with selected fruits, herbs, and natural sweeteners, with the objective of improving its nutritional profile and providing immune-boosting benefits compared to traditional commercial jelly products.

2.MATERIALS AND METHODS

2.1.Purchase of raw materials:

Fruits and vegetables were purchased from the Aljemail city, and the remaining ingredients, such as turmeric, black pepper, honey, and gelatin, were purchased from herbalists and local markets in the Aljemail area.

2.2.Preparation of samples:

Four formulas of jelly candy were prepared for this study. The main ingredients and proportions of samples (1) and (3) were shown in table (1). The ingredients of the two samples are the same, but sample (1) was sweetened by natural bee honey, and sample (3) was sweetened by stevia sugar (to meet the demands of diabetic people and followers of low-calorie, low-carb diets). Firstly, lemon, apple, rosemary, fresh ginger, and mint were washed, removing the outer peels and inner seeds of the lemon and removing the inner seeds of the apples, and adding the remaining ingredients, such as turmeric, black pepper, honey (for sample 1), or stevia (for sample 3). All ingredients were then weighed according to the required proportions shown in table (1) and added to an electric blender and blended for 5 minutes. A plastic strainer was used to filter the juice after it had been blended. Water was placed in a stainless-steel pot, and gelatin was added and dissolved over low heat (about 80°C for 3 minutes) with continuous stirring. The prepared gelatin was then added to the prepared mixture of fruit and herbs and stirred well. The juice was then extracted using a sterilized syringe, poured into silicone molds, and placed in the freezer for at least 10 to 15 minutes.

 ISSN: Online 2790-1637, Print 2790-1629
National Library of Libya, Legal number: 154/2018

Samples (2) and (4) were prepared by washing and peeling pomegranates, carrots, beets, strawberries, lemons, and oranges, removing the inner seeds, and adding the remaining ingredients: turmeric, black pepper, honey (sample 2), or stevia (sample 4). All ingredients were then weighed according to the required proportions shown in table (1) and blended in an electric blender for at least 5 minutes. The juice was blended and then filtered through a plastic sieve. Water was placed in a stainless-steel pot, gelatin was added, and the mixture was dissolved with continuous stirring at a temperature not exceeding a boil just to dissolve the gelatin (about 80°C for 3 minutes). The dissolved gelatin was then added to the juice mixture and stirred well. Then the mixture was taken using a sterile syringe and placed in clean silicone molds and placed in the freezer for at least 10 to 15 minutes.

Note: Halal bovine gelatin powder (Silver) from Amin Gelatin Factories, 6th of October City, Egypt, was used in preparing these samples. Production date: 2024; expiry date: 5 years from the date of production.

Halal commercial jelly candy (HARIBO/made in Türkiye) was used as a control sample.

Table (1): Iingredients and proportion of samples of the jelly candy

Ingredients	Sample (1)	Sample (2)	Sample (3)	Sample (4)
Lemon	11.09%	4.94%	16.43%	5.63%
Apples	33.28%	-	37.91%	-
Ginger	0.44%	0.48%	0.50%	0.169%
Mint	0.44%	-	0.53%	-
Rosemarry	0.26%	-	0.25%	-
Turmeric	0.11%	0.19%	0.12%	0.022%
Blak pepper	0.02%	0.009%	0.03%	0.011%
Pomegranate	-	14.82%	-	16.91%
Beetroot	-	2.47%	-	2.81%
Strawberry	-	19.76%	-	22.55%
Orange	-	19.76%	-	22.55%
Carrots	-	5.93%	-	6.76%
Stevia sugar	-	-	3.79%	2.81%
Hony	18.86%	14.82%	-	-
Gelatine	13.31%	8.40%	15.17%	9.58%
Water	22.19%	8.89%	25.27%	10.198%
Final product	 Sample (1)	 Sample (2)	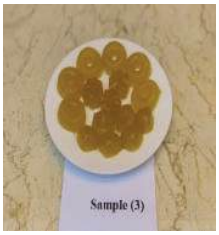 Sample (3)	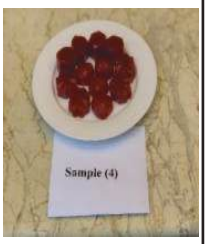 Sample (4)

 ISSN: Online 2790-1637, Print 2790-1629
National Library of Libya, Legal number: 154/2018

2.3.Chemical Analysis:

All chemical and quality analyses were carried out according to approved methods of the Association of Official Analytical Chemists (AOAC 2005).

2.4.Quality analysis:

Total Soluble Solids (T.S.S.) of the juice mixture was determined using a Rhino Brix refractometer HR-150N/ Rhino technology (Brix scale 0-80%). Titerable Acidity: Was determined by the titration method using NaOH (0.1 N) and phenolphthalein as an indicator. PH: PH measurement was conducted using a pH Socket/BNC Socket.

2.5.Proximate Composition:

Moisture content: This was determined using an ATG high-temperature oven (Shanghai/China) at 135 degrees for 2 hours. Ash content: Ash content was determined using a ZE electric muffle furnace (Italy) at 550°C for 6 hours. Protein: This was determined using the micro Kjeldahl method, which includes digestion, distillation, and titration. Fat: This was determined using Soxhlet. Carbohydrate: It was measured using the Anthrone technique as outlined by Plummer (1990). Carbohydrates underwent dehydration using concentrated sulfuric acid (H_2SO_4) to produce furfural. Anthranilic, the enol tautomer of anthrone, was the reagent's active form. It was condensed with the carbohydrate furfural derivative to create a green color in diluted form that could be measured by calorimetry solutions.

2.6.Mineral Analysis:

A flame photometer (BWB Technologies/England) was used in the determination of minerals. For each type of mineral, the concentration was measured against the standard curve.

2.7.Phytochemical Screening:

Phytochemical screening: The technique outlined by Harborne (1998) was used to identify the phytochemical. Polyphenols: This was estimated according to the method of Gutfinger (1981), where the polyphenol compounds were extracted using alcohol (methanolic extract) and then estimated with Folin-Ciocalteau reagent. The extraction was assessed at 695 nm in comparison to the calibration curve. The antioxidant was evaluated through the phosphomolybdenum technique described by Perietop et al. (1999).

2.8.Energy Content:

The energy content was determined via a CALO-3 Bomb calorimeter, which is used to measure the heat of combustion when placed in a reaction container surrounded by water. The temperature of the water surrounding the reaction container rises as the material and oxygen gas are heated until the substance combusts; the combustion temperature is then determined. according to the following equation:

$\Delta U = qv = mcv\Delta T$

where:

• m = mass of water

2.9.Microbiological Analysis:

Compact Dry TC, a quick testing kit designed for measuring aerobic colony counts, coliform, and E. coli, has been developed by Nissui Pharmaceutical Co. for food applications and was used to evaluate the microbial load. The plates are sterilized in advance and contain culture medium, a gelling agent that liquefies in lower temperatures, and a redox indicator that changes color for easier counting (De Vaugelade et al., 2017).

Statistical analysis: All results of this study were subjected to statistical analysis using the SPSS program (version 21) for three replicates and were expressed as mean ± standard deviation.

3.RESULTS AND DISCUSSION

3.1.Quality Analysis:

Table (2) Quality analysis of juice mixture before adding gelatin

Sample	Mean ± SD		
	TSS	Acidity	pH
Sample 1	19.6±0.3	0.09±0.002	3.44±0.00
Sample 2	19.4±0.2	0.05±0.001	3.94±0.02
Sample 3	12.0±0.1	0.10±0.001	3.36±0.01
Sample 4	13.0±0.3	0.04±0.003	3.95±0.02
P-value	<0.001	<0.001	<0.001
Comment	S	S	S

 ISSN: Online 2790-1637, Print 2790-1629
National Library of Libya, Legal number: 154/2018

Table (2) above illustrated the quality properties (TSS, pH, and acidity) of the juice mixture before adding gelatin. Samples 1 and 2, containing natural honey, had higher total soluble solids (TSS) than samples 3 and 4, which contained stevia sugar, indicating that honey played a role in raising TSS. Samples 1 and 3 also exhibited higher acidity and lower pH due to their higher lemon content. With p-values 0.001 below the 0.05 significant level, it was clear that there was a significant difference (at P > 0.05) between samples in the mean of TSS, acidity, and pH. In comparison to previous studies, Basiony et al. (2023), in a study of using pomegranate, beetroot, and strawberry juice to produce yogurt, found that the acidity and pH value of the fresh juice was 4.66±0.01 to 4.75±0.01, and the purée varied from 0.85±0.01 to 1.03±0.01. The results of this study differed from what Basiony et al. (2023) found. This difference may be due to the difference in components and proportions used in this study.

3.2.Proximate Composition:

Table (3) Chemical composition of jelly candy samples (%)

Sample	Mean ± SD					
	Moisture content%	Ash%	Protein%	Fats%	Fibre%	Carbohydrates%
Sample1	68.15±0.005	0.55±0.003	4.76±0.003	3.41±0.01	3.55±0.003	19.58±0.005
Sample2	73.02±0.032	1.87±0.002	6.87±0.009	2.92±0.013	3.02±0.003	12.02±0.003
Sample3	74.85±0.015	0.48±0.004	2.84±0.003	3.75±0.009	2.94±0.006	15.14±0.004
Sample4	79.92±0.034	1.81±0.012	4.91±0.007	2.81±0.003	2.94±0.003	7.61±0.004
Control	5.50±0.007	0±0.001	1.99±0.008	3.98±0.004	2.54±0.002	85.99±0.005
P-value	<0.001	<0.001	<0.001	<0.001	<0.001	<0.001
Comment	S	S	S	S	S	S

One-way ANOVA was used at the 0.05 significant level, with S ≡ significant difference.

Table (3) shows the chemical composition of jelly candy. Sample 1, which consisted of lemon, apple, mint, rosemary, curcumin, black pepper, and honey, had the lowest moisture content and highest fiber and carbohydrate content among the studied jelly candy samples, while the commercial jelly sample had the highest carbohydrate and fat content and lowest moisture content (85.99±0.005, 3.98±0.004, and 5.50±0.007%), respectively. It was noted that the commercial sample was extremely free of ash (0.00), which means that the percentage of minerals and vitamins is very low. From the results shown in the above table, it was also clear that samples 2 and 4, which contained beetroot, pomegranate, and strawberry, were characterized by higher levels of ash and protein (1.87±0.002, 1.81±0.012 and 6.87±0.009, 4.91±0.007%) for honey- and stevia-sweetened samples, respectively. Amer and Abd El-Rhman (2023), in a study aimed at developing a healthy gelatin dessert, found that the protein content of the prepared samples ranged from 2.2 to 3.7% compared to the control sample, which was 7.9%. They also found that the total energy content of the prepared samples ranged from 18.3 to 33.49 kcal/100 g compared to the control sample, which recorded 294 kcal/100 g. Another study aimed to develop a healthy fruit-based gelatin dessert by Teixeira-Lemos et al. (2021) found that the protein content of the prepared samples ranged between 4.04 and 3.25 grams per 100 grams. Sugar content was 8.81 and 4.63 grams per 100 grams, compared to the control sample of 58 grams per 100 grams. Furthermore, the analysis results in the table (3) showed significant differences in the chemical composition of the developed jelly candy compared to the commercial one in terms of carbohydrates, ash (which reflects mineral and vitamin content), and protein. These differences could represent a good advantage to meet the different nutritional and sensory requirements of consumers. Furthermore, it's obvious that the developed jelly candy samples were characterized by their high lev-

 ISSN: Online 2790-1637, Print 2790-1629
National Library of Libya, Legal number: 154/2018

els of dietary fiber (3.55 to 2.94%). Dietary fiber plays a fundamental role in the immune response, as it improves beneficial intestinal microflora, which improves bowel movement. When intestinal microflora ferment dietary fiber, their numbers multiply, thus reducing inflammation and enhancing immunity (Cohen & Elinav, 2023; Yang et al., 2020).

From the results shown in Table (3), the commercial jelly candy contained a very high sugar content and a very low ash content, indicating its low mineral and vitamin levels. Therefore, excessive consumption of commercial jelly candy may negatively affect public health due to their high sugar content and additives, especially colors, as well as their association with tooth decay, high blood sugar, and the risk of obesity. Furthermore, their low nutritional value contradicts the consumer's tendency to consume healthier foods, while the newly developed formulations in this study showed high nutritional value in terms of protein, ash, and fat content and a suitable energy content, especially in the samples sweetened with stevia sugar.

3.3.Total Energy:

Table (4) Total Energy content of jelly candy (kcal/100g)

Sample	Mean ± SD
	Total energy kcal/100g
Sample1	128.06±0.09
Sample2	101.51±0.37
Sample3	105.66±0.07
Sample4	75.74±0.74
Control	387.48±0.39
P-value	<0.001
Comment	S

One-way ANOVA was used at the 0.05 significant level, with S ≡ significant difference.

Table 4 shows the energy contents of the new jelly candy samples compared to the commercial ones. The commercial sample had a very high energy content (387.88±0.39), due to its high carbohydrate content (Table 4), while the improved jelly candy samples showed lower energy contents compared to the commercial sample. As expected, samples sweetened with stevia had the lowest energy content, which makes them a good choice for those following a low-carb diet and diabetics, while the samples sweetened with natural honey showed good levels of energy, making it a suitable healthy choice compared to sweets containing white sugar, according to the health system that many consumers are currently adopting, especially with regard to the calorie content of foods, which may lead to many health disorders (Amer and Abd El-Rhman, 2023). Calder and Kew (2002) indicated that a deficiency in total energy or one or more of the essential nutrients weakens the immune system and increases susceptibility to disease. It is likely that these elements have a fundamental role in the molecular and cellular response of the immune system, and thus the availability of these elements enhances the functions of the immune system's operations and enhances infection resistance.

3.4.Mineral Content:

Table (5) Mineral content of jelly candy (ppm)

Sample	Mean ± SD		
	Sodium	Potassium	Iron
Sample1	9±2	32±2	3±2
Sample2	13±2	64±2	35±2
Sample3	9±1	33±3	3±1
Sample4	11±2	58±1	31±2
Control	25±3	6±0	3±2
P-value	<0.001	<0.001	<0.001
Comment	S	S	S

One-way ANOVA was used at the 0.05 significant level, with S ≡ significant difference.

Table (5) showed the percentage of minerals (ppm) in jelly candy samples. Samples 2 and 4, containing beetroot, strawberry, and pomegranate, were distinguished by their higher levels of sodium, potassium, and iron among the samples prepared in this study, while the control sample showed the highest level of sodium and the lowest levels of both potassium and iron. The control sample contained the highest sodium level (25 ppm), and sample 2 had the highest potassium level (64), and sample 3 had

the highest iron level (35 ppm). Amer & Abd El-Rhman (2023) found that the percentage of iron, sodium, and potassium in samples of jelly sweets prepared from some fruits ranged between Fe: 8.25 to 10.05, Na: 35.3 to 90.3, and K: 1191 to 1229 mg/100 g, respectively, while the control sample recorded percentages of 5.16, 10.9, and 780.3 for the same elements, respectively. Minerals were important micronutrients linked to numerous aspects of human health (Amer & Abd El-Rhman, 2023). For example, potassium played a key role in insulin resistance and type 2 diabetes, according to the U.S. Department of Agriculture (2020-2025), while iron is crucial for preventing anemia and aiding children's growth (Wang et al., 2019). The immune system needs minerals such as iron, zinc, and magnesium, which participate with vitamins A and D in the synthesis of nucleotides and nucleic acids (DNA and RNA), which are regulators of the genetic sequence of immune cells and play an important role in the maturation and response of immune cells (Calder, 2013).

3.5.Phytochemical Analysis:

Table (6) Phytochemical screening for jelly candy

	Sample 1	Sample 2	Sample 3	Sample 4	Control
Flavonoid	+++	-ve	+++	++	+
Phenols	++	+++	+++	+++	+
Alkaloids	-ve	-ve	-ve	-ve	+++
Glycosides	+++	+++	+++	+++	+++
Saponin	+++	+++	+	+	-ve
Tannins	+++	+++	+++	+++	+

-ve Negative +weak ++ medium +++ strong

Table (6) showed the initial screening of active chemical compounds in the new jelly candy samples compared to commercial jelly candy. The results showed that the manufactured gelatine candy samples were richer in phenols, glycosides, and tannins than the commercial sample. It is also noted that the samples sweetened with natural honey had the highest saponin content. The commercial sample was low in flavonoids, phenols, and tannins; did not contain saponins; and had a high content of alkaloids and glycosides. Many previous studies had focused on developing jelly sweets by adding fruits, medicinal herbs, and propolis, which are rich in antioxidants and active phytochemicals (Al-Jaloudi et al., 2025; Roudbari et al., 2024; Tarahi et al., 2024; Masri, 2023).

Table (7) Polyphenols and antioxidant

Sample	Mean ± SD	
	Polyphenols(mg/QE/g)	Antioxidants(mg/GAE/g)
Sample1	111.1±13.91	0.09±0.06
Sample2	135.64±4.36	0.19±0.012
Sample3	120.68±5.98	0.07±0.011
Sample4	131.98±20.39	0.09±0.022
Control	0.94±1.4	0.05±0.001
P-value	<0.001	0.002
Comment	S	S

One-way ANOVA was used at the 0.05 significant level, with S ≡ significant difference.

Table (7) showed the content of polyphenols and antioxidant activity of the improved jelly candy samples. It is clear from the table above that the prepared samples were rich in polyphenols, especially samples (2,4) containing beetroot, pomegranates, and strawberries; this may be due to these items being rich in these compounds, which makes them the best combination in terms of active chemical compounds compared to the control sample (commercial jelly candy), which was

very poor in polyphenols and antioxidant activity. The above table also shows that there is a significant difference between the samples in the mean of polyphenols and antioxidants (p-values are 0.001). Rubio-Arraez et al. (2018) found that the antioxidant activity values of jelly samples in which sugar was replaced by other sweeteners were found to range from 8.3 to 9.9 mg/100 g. In another study, Teixeira-Lemos et al. (2021) prepared gelatin desserts from orange, honey, and mixed berries. It was found that both samples had antioxidant capacity, while the mixed berry dessert was distinguished by higher antioxidant activity. Compared to the findings of the current study, the antioxidant capacity of the prepared samples was significantly lower than that reported in the two previous studies. This may be due to the differences in the components and their composition in the prepared gelatin desserts.

3.6.Sensory Evaluation:

Table (8) Sensory evaluation

Sample	Mean ± SD			
	Colour	Taste	Flavour	Over all acceptability
Sample1	4.13±1.049	2.30±0.997	2.33±1.284	2.65±1.022
Sample2	4.27±0.989	2.82±1.049	2.65±1.117	3.28±1.059
Sample3	4.50±0.911	3.75±1.174	3.72±1.151	4.07±1.133
Sample4	4.65±0.840	4.28±0.885	4.27±0.821	4.53±0.791
P-value	0.015	<0.001	<0.001	<0.001
Comment	S	S	S	S

Two independent sample t-tests were used at the 0.05 significance level. If the p-value < 0.05 (significant difference), then the mean is 4.21 to 5 (excellent), 3.41 to 4.2 (very good), 2.61 to 3.4 (acceptable), or less than 2.61 (not acceptable).

Table (8) showed the results of the sensory evaluation of the new jelly candy samples. The evaluators preferred the samples sweetened with stevia sugar over the samples sweetened with natural honey in all the sensory attributes tested (color, taste, flavor, and overall acceptability). The evaluation also revealed that the evaluators preferred Sample 4, which contained beetroot, pomegranate, and strawberry sweetened with stevia sugar, over all the prepared samples. The table also shows that there are significant differences at 0.05 between the prepared samples. Commercial jelly candy is poor in nutrients (Tiwari & Rastogi, 2024). However, compared to the improved jelly candy in this study, it was found more acceptable. With the currently developed jelly candy, the consumer would obtain formulas with improved nutritional and sensory properties, in addition to their low sugar content. In general, consumer acceptance of candy is affected by its consistency. The lower the consistency of the candy, the easier it is to chew and swallow.

3.7.Microbiological Analysis:

Table (9) Microbiological analysis (CFU/100gm) 10^2

Samples	Sample 1	Sample 2	Sample 3	Sample 4	Control
Total count	2	5	2	5	Nill
Coliforms	Nill	Nill	Nill	Nill	Nill
E. coli	Nill	Nill	Nill	Nill	Nill

Table (9) shows the microbial analysis of the prepared jelly candy samples compared to the commercial sample. The results showed that the total microbial count in the prepared samples did not exceed 5 cell-forming units, while all samples were free of coliform bacteria and Escherichia coli. The control sample (commercial) was free of microbial contaminants. In a study on the manufacture of fruit-based jelly sweets, the results showed that both prepared samples showed aerobic growth (1 and 1.3×102 CFU) (Teixeira-Lemos et al., 2021), which is lower than the limits permitted in European Union legislation (ICMSF, 2005) (<103 CFU). In comparison, the number of colony-forming units was observed to be lower in the jelly sweets manufactured in this study, which means that they are microbially safe for human

 ISSN: Online 2790-1637, Print 2790-1629
National Library of Libya, Legal number: 154/2018

consumption.

4.CONCLUSION

This study demonstrated the successful development of jelly candy formulated with natural, immune-boosting ingredients. The produced samples showed nutritional advantages over traditional commercial candy, particularly in their higher protein, fiber, antioxidant activity, and potassium levels. The current study provided a future vision for utilizing fruits, vegetables, and aromatic herbs with immune-boosting components such as turmeric, ginger, and black pepper in new applications of high nutritional and health value, as demonstrated by the high percentage of protein, fiber, and chemically active plant compounds in improving jelly candy samples. This jelly candy had significant potential as an attractive, health-beneficial functional food product. Overall, the findings indicated that the formulated jelly candies provide enhanced nutritional quality, valuable bioactive compounds, and favorable sensory properties, positioning them as promising functional food products. These results supported the potential for developing a functional confectionery industry based on natural ingredients rich in macro- and micronutrients and phytochemicals.

5.COMPETING INTEREST

The authors had no relevant financial information to disclose.

6,FUNDING

The authors declared that no funding grant or other support was received during the preparation of this manuscript.

7.ACKNOWLEDGMENT

The authors would like to extend their sincere gratitude to the people who agreed to taste the developed jelly candy formulations and provide their opinions and feedback.

REFERENCES

1.Abdallah, H. M., Abu Al khararib, T. K., Al koudi, K. A. (2023). Innovation of a new milk drink using natural immune-boosting ingredients. Journal of Saudi Society for Food and Nutrition. 16(1), 48-59.

2.Al-Jaloudi, R., Al-Refaie, D., Shahein, M., Hamad, 3.H. J., Al-Dabbas, M. M., Shehadeh, N., AlBtoosh, J., Al-Nawasrah, B. A., Alkhderat, R., & Ababneh, S. K. (2025). Development of Functional Jelly Gums Using Blueberry Concentrate and Honey: Physicochemical and Sensory Analysis. Processes, 13(2), 508. https://doi.org/10.3390/pr13020508

4.Amer, S.A., and Abd El-Rahman H. S. M. (2023) Development and evaluation of free sugar jelly made with leafy vegetables as a functional food. Carpathian journal of food science and technology. https://doi.org/10.34302/crpjfst/2023.15.3.3.

5.AOAC (2005) Official Methods of Analysis of the Association of Official's Analytical Chemists. 18th Edition, Association of Official Analytical Chemists (AOAC), Arlington, Virginia.

6.Basiony, M., Saleh, A., Hassabo, R. et al. (2023). The effect of using pomegranate and strawberry juices with red beet puree on the physicochemical, microbial and sensory properties of yoghurt. Food Measure 17, 5024-5033. https://doi.org/10.1007/s11694-023-01984-8.

7.Burey, P., Bhandari, B. R., Rutgers, R. P. G., Halley, P. J., & Torley, P. J. (2009). Confectionery gels: A review on formulation, rheological and structural aspects. International Journal of Food Properties, 12(1), 176-210. https://doi.org/10.1080/10942910802223404.

8.Calder, P. C., & Kew, S. (2002). The immune system: a target for functional foods? The British journal of nutrition, 88 Suppl 2, S165-S177. https://doi.org/10.1079/BJN2002682 PMid:12495459.

9.Cohen, Y., & Elinav, E. (2023). Dietary fibers & immunity-more than meets the eye. Cell Research, 2-3. https://doi.org/10.1038/s41422-022-00770-3 PMid:36646763 PMCid: PMC10235049.

10.De Vaugelade, S., Aime, M., Farcette, N., Maurel, E., Lacour, T., Thomas, C., Bouchonnet, S., & Pirnay, S. (2017). Comparison of the compact dry TC method with the standard method ISO 21149:2006 for determining aerobic colony counts in cosmetic emulsion. International journal of cosmetic science, 39(1), 17-24. https://doi.org/10.1111/ics.12343 PMid:27189374

11.Devirgiliis, C., Guberti, E., Mistura, L., & Raffo, A. (2024). Effect of Fruit and Vegetable Consumption on Human Health: An Update of the Literature. Foods, 13(19), 3149. https://doi.org/10.3390/foods13193149 PMid:39410184 PMCid: PMC11475733

12.Gasmi, A., Shanaida, M., Oleshchuk, O., Semenova, Y., Mujawdiya, P. K., Ivankiv, Y., Pokryshko, O., Noor, S., Piscopo, S., Adamiv, S., & Bjørklund, G. (2023). Natural Ingredients to Improve Immunity. Pharmaceuticals, 16(4), 528. https://doi.org/10.3390/ph16040528. PMid:37111285 PMCid: PMC10143734

13.Gutfinger, T. (1981). Polyphenols in olive oil. Journal of the American Chemists society. Volume 58. Issue 11/ pages 966-968.https://doi.org/10.1007/BF02659771

14.Harborne, J. B. (1998). Phytochemical methods/ A guide to modern techniques in plant analysis/ 3ed edition. Published by Chapman & Hall, an imprint of Thornson Science, 2-6 Boundary Row, London SE18HN, UK.

15.ICMSF. Microorganisms in foods. New York, USA: Kluwer Academic/Plenum Publishers; 2005.

16.Luo Y, Li Y, Dai J, (2020). Low blood sodium increases risk and severity of COVID-19: a systematic review, meta-analysis and retrospective cohort study. Med Rix. https://doi.org/10.1101/2020.05.18.20102509

17.Marfil, P. H. M. , Anhê, A. C. B. M. , & Telis, V. R. N. (2012). Texture and microstructure of gelatin/corn starch-based gummy confections. Food Biophysics, 7, 236-243.https://doi.org/10.1007/s11483-012-9262-3

18.MasriA.A, Bakar F.I.A, Abidin M.Z, Malik N.H. (2023). Development of Antioxidant Jelly Using Tropical Fruits. Trop J Nat Prod Res. 2023; 7(7):3433-3438 http://www.doi.org/10.26538/tjnpr/v7i7.22. https://doi.org/10.26538/tjnpr/v7i7.22

19.Prietop, Pineda M, AguilarM. (1999). Spectrophotometeric quantitation of antioxidant capacity through the formation of a phosphomolybdenum complex specific application to the Determination of vitamin. E Anal Biochem, 1999;269, 337-341.https://doi.org/10.1006/abio.1999.4019. PMid:10222007

20.Roudbari, M., Barzegar, M., i Sahari, M. A., Gavlighi, H. A. (2024). Formulation of functional gummy candies containing natural antioxidants and stevia. Heliyon. Volume 10, Issue 11, 15 June 2024, e31581. https://doi.org/10.1016/j.heliyon.2024.e31581. PMid:38841479 PMCid: PMC11152653

21.Rubio-Arraez S, Benavent C, Ortolá MD, Castelló ML. Influence of low glycaemic index sweeteners on antioxidant, sensory, mechanical, and physicochemical properties of a watermelon jelly. J Food Qual. 2018;2018. https://doi.org/10.1155/2018/8412017

22.Singh, D. N., Bohra, J. S., Dubey,T. P., Shivahre, P. R., Singh, R. K., Singh, T., Jaiswal,D. K. (2023). Common foods for boosting human immunity: A reviewFood science and nutrition, Volume11, Issue11 November 2023 Pages 6761-6774. https://doi.org/10.1002/fsn3.3628 PMid:37970422 PMCid:PMC10630845

23.Tarahi, M., Tahmouzi, S., Kianiani, M. R., Ezzati, S., Hedayati, S., & Niakousari, M. (2024). Current Innovations in the Development of Functional Gummy Candies. Foods, 13(1), 76. https://doi.org/10.3390/foods13010076. PMid:38201104 PMCid: PMC10778822

24.Teixeira-Lemos, E., Almeida, A., Vouga, B., Morais, C., Correia, I., Pereira, P. & Guiné, R. (2021). Development and characterization of healthy gummy jellies containing natural fruits. Open Agriculture, 6(1), 466-478. https://doi.org/10.1515/opag-2021-0029

25.Tiwari, D., Rastogi, M. (2024). Gummy Jellies: Properties and Advancements. International Journal of Plant Biotechnology. 2024; 12(3): 21-34p.

26.U.S. Department of Agriculture and U.S. (202-2025). Department of Health and Human Services. Dietary Guidelines for Americans, 2020-2025. 9th ed. Washington, DC: US Government Publishing Office; 2020. DietaryGuidelines.gov.

27.Vishwakarma, S. , Panigrahi, C. , Barua, S. , Sahoo, M. , & Mandliya, S. (2022). Food nutrients as inherent sources of immunomodulation during COVID-19 pandemic. LWT - Food Science and Technology, 158, 113154.https://doi.org/10.1016/j.lwt.2022.113154.

PMid:35125518 PMCid: PMC8801482

28.Yang, H., Sun, Y., Cai, R., Chen, Y., & Gu, B. (2020). The impact of dietary fiber and probiotics in infectious diseases. Microbial Pathogenesis, 140(September 2019), 103931. https://doi.org/10.1016/j.micpath.2019.103931. PMid:31846741

29.Wang, Y., Wu, Y., Li, T., Wang, X., & Zhu, C. (2019). Iron metabolism and brain development in premature infants. Frontiers in Physiology, 10, 463. https://doi.org/10.3389/fphys.2019.00463. PMid:31105583 PMCid: PMC6494966

 ISSN: Online 2790-1637, Print 2790-1629
National Library of Libya, Legal number: 154/2018

Scientific Journal of University of Benghazi

SJUOB (2025) 38 (2) Medical Sciences: Altawati. et.al., 126 – 138
www.sjuob.uob.edu.ly

Prevalence of Glaucoma in Patients Attending Glaucoma Screening Program: A Cross-Sectional Study, Benghazi, Libya.

Rehab S. Altawati [1]*, Nada A. Elsaeid [1], Samar A. Bukhatwa [1].

1.Ophthalmology Department, Faculty of Medicine, University of Benghazi/ Libya.

DOI: 10.37376/sjuob.v38i2 | Received:18/09/2025 | Accepted:07/11/2025 | Publishing: 23/12/2025

ABSTRACT

Glaucoma, a leading cause of blindness worldwide, glaucoma afflicted 64.3 million people in 2013 and is expected to affect 111.8 million by 2040. For early detection and treatment, it is essential to look into the prevalence of glaucoma and its risk factors. Finding important clinical and demographic indicators of glaucoma in adults screened as part of a public program in Benghazi, Libya, was the goal of this study. During "Glaucoma Week" in February 2024, 366 adult patients were recruited for this cross-sectional study. The participants were divided into three categories: glaucoma suspect (21.0%, n=77), glaucoma unlikely (34.5%, n=126), and confirmed glaucoma (44.5%, n=163). A first-degree relative with glaucoma (OR =2.08, p = 0.016), a history of ocular inflammation (OR = 5.2; p = 0.008), and a higher left-eye intraocular pressure (IOP) (OR = 1.18, p = 0.003) were all significant predictors of confirmed glaucoma, according to logistic regression analyses. In one model, male gender was also a significant predictor (OR = 1.85, p = 0.027). The development of glaucoma was significantly influenced by these factors. In order to improve glaucoma detection in Libya, this study highlighted the significance of targeted screening and monitoring, especially for people with ocular inflammation, a family history of glaucoma, or elevated left-eye IOP.

KEYWORDS: screening, glaucoma suspicion, blindness, inflammation, intraocular pressure, Libya.

Corresponding Author: Rehab S Altawati, *rehab.altawati@uob.edu.ly*

 ISSN: Online 2790-1637, Print 2790-1629
National Library of Libya, Legal number: 154/2018

1.INTRODUCTION

Glaucoma causes progressive damage to the optic nerve and visual fiel,[1,] is the second most common cause of permanent blindness worldwide, after cataracts. [2,3] It is responsible for more than 8% of blindness globall,[4] and the number of cases is predicted to rise from 64.3 million in 2013 to 111.8 million in 2040.[5]

Glaucoma is associated with high intraocular pressure (IOP), and risk factors include age, IOP, race, gender, and family history.[6] Glaucoma affects about 4% of adults over the age of 40 in Sub-Saharan Africa; however, limited diagnostic resources frequently result in underreporting and delayed diagnosis. Many cases go undiagnosed until advanced stages, highlighting the necessity of extensive screening programs.[3]

In Libya, data on prevalence and associated risk factors are particularly limited, making it difficult to develop effective screening and prevention strategies. Given the disease's high risk and the importance of early intervention,[7] a targeted screening approach is required to identify and manage high-risk individuals in the Libyan population. Research into the prevalence and associated risk factors of glaucoma is critical for early detection and a better understanding of its pathophysiology [8].

Therefore, the purpose of this study was to determine important clinical and demographic risk factors as well as the prevalence of glaucoma among adults participating in a screening program in Benghazi. The study would fill a significant knowledge gap in the field of ophthalmic epidemiology in Libya and advances evidence-based strategies for early detection and treatment.

2.MATERIALS AND METHODS

A cross-sectional study was carried out at the outpatient department of the Benghazi Teaching Eye Hospital. In collaboration with the ophthalmology department at the University of Benghazi, the hospital organized a glaucoma screening event called "Glaucoma Week," which took place during the last week of February 2024.

Patients were invited to participate through advertisements in local news media. The study included all adult patients who visited the outpatient department at the study site during this week and consented to participate in the screening program. However, participants with corneal surface disease, phthisis, or those unable to fixate were excluded from the study. Adult patients attending the outpatient department that week, recruited via local news ads and giving consent, were included. Participants with corneal surface disease, phthisis, or inability to fixate were excluded from the study.

Demographic, medical, and eye health information, including age, gender, race, glaucoma and other eye disease histories, prior treatments, family glaucoma history, medication use, systemic diseases (heart disease, stroke, hypertension, diabetes), and smoking, was recorded in a database by volunteer ophthalmologists.

During the screening examination, the following parameters were assessed: Visual acuity, refraction, and intraocular pressure (IOP). Myopia was characterized as a spherical equivalent (SE) of ≤ –0·5 diopters [9], and normal IOP was defined as a range of 10 to 21 mmHg. [10] A comprehensive ocular examination was conducted, which included slit-lamp bio-microscopy and a fundus examination with a (+90D) lens to evaluate the optic nerve head.

Each patient was categorized into one of the three groups based on clinical and historical findings: Confirmed glaucoma was diagnosed if classic optic neuropathy (optic disc cupping/ damage) appeared in either eye, irrespective of visual field-testing results, and was validated by medical record review. [11]

Glaucoma suspect was classified as an individual presenting with clinical features or risk factors that increase the risk of glaucoma-related optic nerve damage. [11,12]

Glaucoma unlikely was defined as a patient with IOP below 21 mmHg, a normal appearance of the optic disc, and no family history of glaucoma in a first-degree relative. [11]

Patients were informed of their results and scheduled for follow-up after examination. Multinomial and binary logistic regression assessed associations between glauco-

 ISSN: Online 2790-1637, Print 2790-1629
National Library of Libya, Legal number: 154/2018

ma diagnosis (confirmed vs suspected, or no glaucoma) and predictor variables, with significance set at $p < 0.05$. The study followed the Declaration of Helsinki and was approved by the Ophthalmology Department and Benghazi Teaching Eye Hospital ethics committees.

3.RESULTS

Out of the 366 participants, specifically 211 (57.7%) were aged over 60 years, 218 (59.6%) were male, 343 (93.7%) were White, and 351 (95.9%) were Libyan. In terms of clinical characteristics, 60 (16.4%) were current smokers, 176 (48.1%) had diabetes, 148 \ (40.4%) had hypertension, 51 (13.9%) had ischemic heart disease, and 92 (25.1%) reported migraines (see Figure 1).

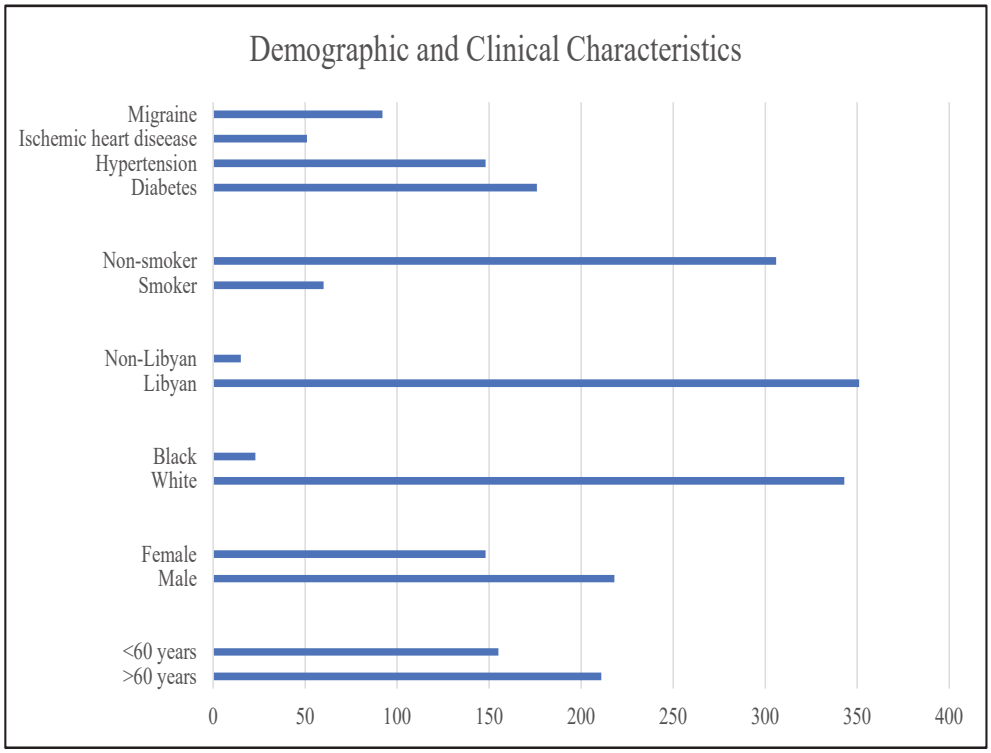

Figure 1. Demographic and Clinical Characteristics (N = 366).

A total of 137 individuals (37.4%) reported no history of ocular conditions. Conversely, 42 (11.5%) had experienced ocular trauma, and 26 (7.1%) had a history of inflammation. Ocular surgery was reported by 108 participants (29.5%), primarily cataract surgery. (Figure 2).

 ISSN: Online 2790-1637, Print 2790-1629
National Library of Libya, Legal number: 154/2018

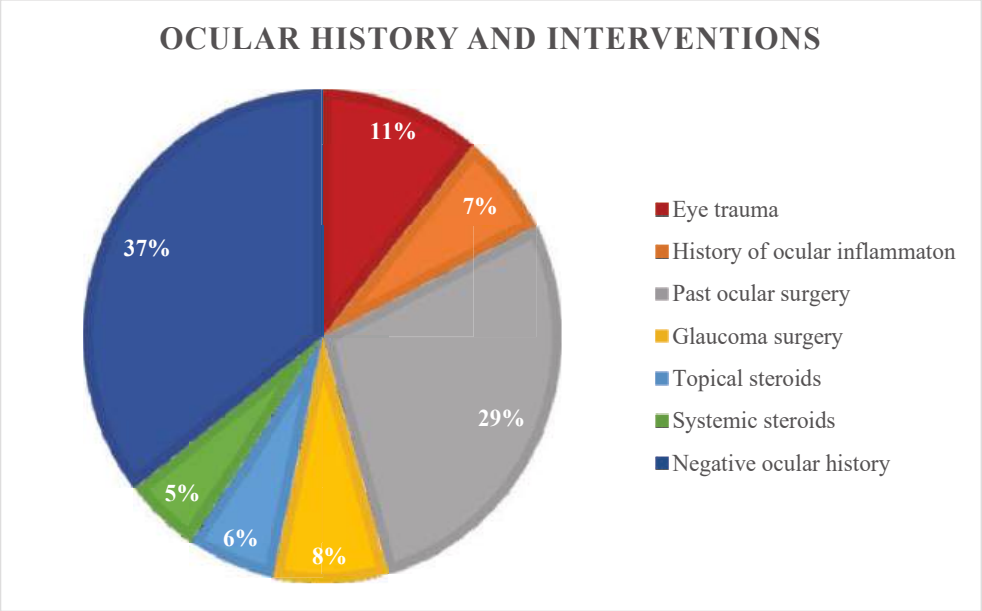

Figure 2: Ocular History and Interventions among Study Participants

Among the 366 studied participants, 163 (44.5%) were confirmed to have glaucoma, 77 (21.0%) were identified as glaucoma suspects, and 126 (34.4%) were considered unlikely to have the disease (Figure 3).

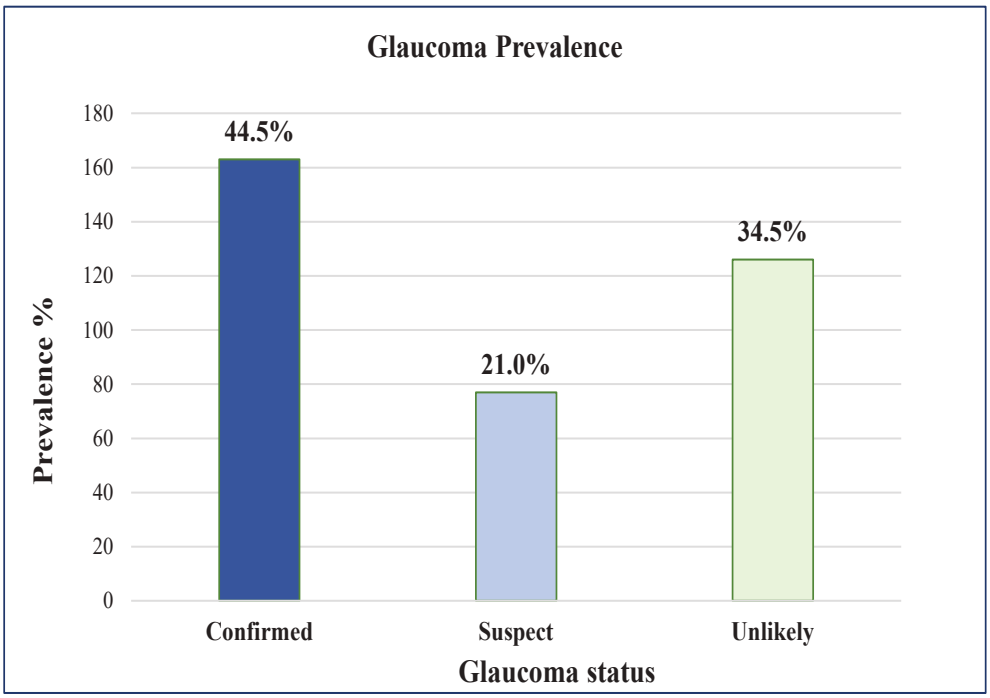

Figure 3. The prevalence of glaucoma status among 366 participants.

 ISSN: Online 2790-1637, Print 2790-1629
National Library of Libya, Legal number: 154/2018

Of the participants, 130 (35.5%) reported a family history of glaucoma, with 120 (32.8%) having a first-degree relative affected. Half of the participants, 183 (50.0%), were myopic.

For glaucoma diagnosis duration, 62 (16.9%) had a duration of more than five years,

Regarding glaucoma treatment, 203 participants without a prior history of glaucoma (55.4%) did not receive any specific intervention, and 137 (37.5%) were treated with drops and tablets (see Table 1).

Table 1: Glaucoma History, Familial Predisposition, and Management Approaches Among Study Participants

Glaucoma	Level	Frequency
Family history of glaucoma	No history	236 (64.5%)
	First-degree relative	120 (32.8%)
	Second-degree relative	9 (2.5%)
	3rd-degree relative	1 (0.3%)
Myopic	—	183 (50.0%)
Glaucoma history	No glaucoma	203 (55.4%)
	Less than 1 year	47 (12.8%)
	1–5 years	42 (11.5%)
	More than 5 years	62 (16.9%)
	Don't know	12 (3.4%)
Treatment	No glaucoma	203 (55.4%)
	Drops and tablet	137 (37.5%)
	Laser	3 (0.8%)
	Combination of Laser, drops and tablet	2 (0.5%)
	Surgery combined with laser	1 (0.3%)
	Surgery combined with drops	11 (3.0%)
	Laser combined with drops	9 (2.5%)

Males were frequently categorized as "suspect" for glaucoma (49 cases, 63.6%), while females represented a higher portion of confirmed cases (71 cases, 43.6%). Despite these differences, sex was not significantly linked to glaucoma status ($p = 0.52$), suggesting that sex is not a significant predictor of glaucoma diagnosis in this group. Most participants in all glaucoma categories were White (151 cases, 92.6%). There was no significant association between race and glaucoma status ($p = 0.41$).

Age significantly correlated with glaucoma ($p = 0.003$); confirmed cases rose with age, about 36.8% (60 cases) in ages 61–70 and 16.0% (26 cases) in ages 71–80. This trend suggests that older age markedly increases glaucoma risk (Refer to Table 2).

Table 2: Distribution of Glaucoma Status by Sex, Race, and Age Group

	Glaucoma status			
	Unlikely	**Suspect**	**Confirmed**	**p-value**
Sex				0.518
Male	77 (61.1%)	49 (63.6%)	92 (56.4%)	
Female	49 (38.9%)	28 (36.4%)	71 (43.6%)	
Race				0.413
White	121 (96.0%)	71 (92.2%)	151 (92.6%)	
Black	5 (4.0%)	6 (7.8%)	12 (7.4%)	
Age Group				0.003*
20-30	2 (1.6%)	1 (1.3%)	6 (3.7%)	
31-40	3 (2.4%)	2 (2.6%)	7 (4.3%)	
41-50	28 (22.2%)	13 (16.9%)	22 (13.5%)	
51-60	48 (38.1%)	38 (49.4%)	40 (24.5%)	
61-70	36 (28.6%)	19 (24.7%)	60 (36.8%)	
71-80	9 (7.1%)	3 (3.9%)	26 (16.0%)	
>80	0 (0.0%)	1 (1.3%)	2 (1.2%)	

$p < 0.05$ = Statistically significant (marked with *). Confirmed glaucoma cases had much higher average ranks for both right (117.14) and left (114.13) optic disc cups than suspect cases, with both differences highly significant ($p < 0.001$). This suggests a strong link between increased optic disc cupping and glaucoma severity (Table 3).

Table 3: Comparison of Optic Disc Cup and IOP Between Glaucoma Suspect and Confirmed Cases

Parameter	Glaucoma Status	N	Mean Rank	p-value
Right Optic Disc Cup	Suspect	66	67.99	<0.001*
	Confirmed	135	117.14	
	Total	201		
Left Optic Disc Cup	Suspect	64	68.86	<0.001 *
	Confirmed	134	114.13	
	Total	198		
Right IOP (Goldmann Applanation Tonometer)	Suspect	70	101.53	0.555
	Confirmed	139	106.75	
	Total	209		
Left IOP (Goldmann Applanation Tonometer)	Suspect	67	98.06	0.404
	Confirmed	138	105.40	
	Total	205		

* Statistically significant results ($p < 0.05$)

Mean IOP ranks measured by Goldmann Applanation Tonometer were slightly higher in confirmed glaucoma cases than suspects for both eyes, but differences were not statistically significant (Table 3).

Multinomial logistic regression showed that only left eye IOP significantly predicted glaucoma diagnosis (p = 0.003; OR: 1.18, 95% CI: 1.06–1.31), representing an 18.2% increase in odds per unit. (see Table 4).

Table 4: Multinomial Logistic Regression Findings

Category	Odds Ratio	95% CI Lower	95% CI Upper	p-value
Constant	0.02	0.003	0.16	<0.001*
Age	1.01	0.98	1.03	0.329
Gender	1.57	0.86	2.84	0.136
Race	2.06	0.54	7.74	0.285
Right Optic Disc Cup (REODcup)	1.00	0.99	1.002	0.962
Left Optic Disc Cup (LEODcup)	0.99	0.99	1.001	0.563
Right IOP (REIOP by Goldmann)	1.04	0.94	1.14	0.426
Left IOP (LEIOP by Goldmann)	1.18	1.06	1.31	0.003*

$p < 0.05$: Statistically significant (marked with *).

Older adults, particularly those aged 61–80 and above 80, show higher glaucoma rates of glaucoma, with narrow confidence intervals indicating strong statistical reliability. Elevated glaucoma rates are also associated with larger cup-to-disc ratios (0.71–1.0). In some groups, wider confidence intervals reflect greater variability in estimates. IOP over 30 mmHg is associated with an increased risk of glaucoma, but has more uncertainty (wider confidence intervals), whereas IOP in the range of 11–20 mmHg provides the most reliable estimates (see Figure 4).

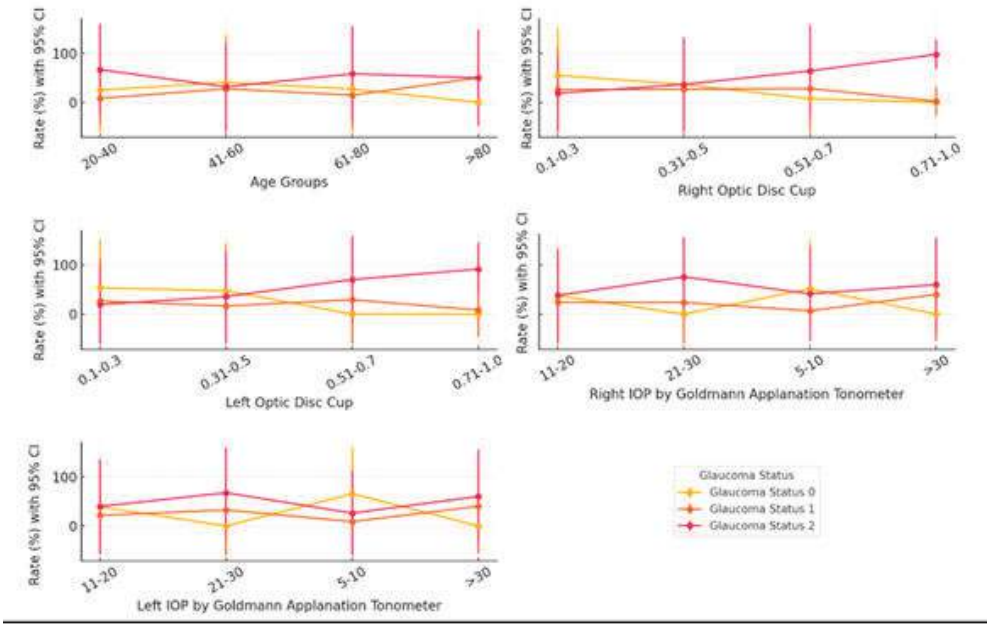

Figure 4: Categorical Risk Plot with 95% Confidence Intervals for Glaucoma Status.

Each subplot illustrates a single predictor variable: Age, Optic Disc Cup, and IOP.

The X-axis displays various categories of the predictor variable.

The Y-axis displays the percentage of individuals in each category corresponding to specific glaucoma statuses: 0 = No Glaucoma, 1 = Suspect, and 2 = Confirmed.

Lines with markers: Indicate the trend of glaucoma risk across categories.

Error bars (95% Confidence Interval (CI)): Represent the confidence level of the rate estimates

According to Model 1 of the binary logistic regression analysis (see Table 5), previous ocular inflammation increased the risk of developing glaucoma by fivefold (OR = 5.2, p = 0.008; 95% CI: 1.53–17.58). Additionally, individuals with a first-degree relative who had glaucoma have a doubled risk (OR = 2.08, p = 0.01; 95% CI: 1.14–3.78). Higher left-eye intraocular pressure (IOP) was another significant factor (OR = 1.10, p = 0.020; 95% CI: 1.02–1.20), where each unit increased in IOP raised the glaucoma risk by 10.3%.

Table 5: Binary Logistic Regression Results for Glaucoma Diagnosis (Model 1: the glaucoma diagnosis adjusted for Age, Gender, Race, Diabetes, Hypertension, Migraine, History of Eye Trauma, History of eye inflammation, Smoking, Ischemic Heart Disease, Family History of Glaucoma, Right Optic Disc Cup, Left Optic Disc Cup, Right IOP, Left IOP)

Variable	Odds Ratio	95% CI Lower	95% CI Upper	p-value
Constant	0.02	-	-	<0.001*
Age	1.02	0.99	1.05	0.07
Gender (Male)	1.83	0.99	3.39	0.05
Race (White)	1.66	0.57	4.78	0.34
Diabetes (Yes)	0.73	0.40	1.35	0.32
Hypertension (Yes)	0.67	0.34	1.31	0.24
Migraine (Yes)	0.87	0.43	1.75	0.70
History of Eye Trauma (Yes)	1.03	0.39	2.76	0.93
History of inflammation (Yes)	5.19	1.53	17.57	0.008*
Smoking (Yes)	1.21	0.49	2.97	0.67
Ischemic Heart Disease (Yes)	1.48	0.61	3.54	0.37
Family History of Glaucoma	-	-	-	-
Family History (Degree 1)	2.08	1.14	3.78	0.01*
Family History (Degree 2)	1.34	0.25	7.03	0.72
Right Optic Disc Cup	1.00	0.99	1.00	0.61
Left Optic Disc Cup	0.99	0.99	1.00	0.38
Right IOP	1.01	0.93	1.09	0.76
Left IOP	1.10	1.01	1.19	0.02*

$p < 0.05$ indicates a statistically significant predictor (marked with *).

Model 2 (Table 6) indicated that males were 85.3% more likely than women to be diagnosed with glaucoma ($p = 0.02$, OR = 1.85). Additionally, a higher left eye IOP was also significantly associated with an increased risk of glaucoma ($p = 0.003$, OR = 1.09); for each unit rise in left eye IOP the risk grows by 9.7%.

Although age slightly increased the odds of developing glaucoma, this association was not statistically significant ($p = 0.154$, OR = 1.01, 95% CI: 0.99–1.04).

Table 6: Binary Logistic Regression Results for Glaucoma Diagnosis (Model 2: the glaucoma diagnosis adjusted for Age, Gender, Race, Right Optic Disc Cup, Left Optic Disc Cup, Right IOP, Left IOP)

Variable	Odds Ratio	95% CI Lower	95% CI Upper	p-value
Constant	0.03	-	-	<0.001*
Age	1.01	0.99	1.04	0.15
Gender (Male = 1)	1.85	1.07	3.20	0.02*
Race (Non-White = 1)	1.56	0.57	4.26	0.38
Right Optic Disc Cup	1.00	0.99	1.00	0.80
Left Optic Disc Cup	0.99	0.99	1.00	0.56
Right IOP	1.00	0.97	1.04	0.65
Left IOP	1.09	1.03	1.16	0.003*

$p < 0.05$ = Statistically significant (marked with *).

Model 3 (Table 7) showed that having a history of ocular inflammation significantly raised the risk of developing glaucoma (OR = 2.82, $p = 0.02$, 95% CI: 1.17–6.76).

Table 7: Binary Logistic Regression Results for Glaucoma Diagnosis (Model 3: History of Eye Trauma, History of Ocular Inflammation, Myopia)

Variable	Odds Ratio	95% CI Lower	95% CI Upper	p-value
Constant	0.66	-	-	0.00*
History of Eye Trauma (Yes)	1.19	0.61	2.32	0.60
History of ocular inflammation (Yes)	2.82	1.17	6.76	0.02*
Myopia (Yes)	1.21	0.79	1.84	0.36

$p < 0.05$ = Statistically significant (marked with *).

Table 8 provided a comprehensive summary of the findings from the three binary logistic regression models, highlighting the factors associated with glaucoma diagnosis.

Table 8: (Summary Table) Predictors of Glaucoma Diagnosis

Predictor	Model 1	Model 2	Model 3	Overall
Left Eye IOP	√	√	—	Strong Risk Factor
Ocular Inflammation	√	—	√	Strong Risk Factor
First-Degree Relative with Glaucoma	√	—	—	Risk Factor
Gender (Male)	X	√	—	Risk Factor
Age	X	X	—	No clear effect
Race	X	X	—	No clear effect
Right Eye IOP	X	X	—	No effect
Optic Disc Cupping	X	X	—	No effect
Eye Trauma	X	—	X	No effect

 ISSN: Online 2790-1637, Print 2790-1629
National Library of Libya, Legal number: 154/2018

Predictor	Model 1	Model 2	Model 3	Overall
Myopia	—	—	X	No effect
Other Medical Histories (Diabetes, HTN, Smoking, etc.)	X	—	—	No effect

√ Significant finding, X Not significant, — Not included in the model

4.DISCUSSION

The study identified a relatively high prevalence of glaucoma in adults screened in Benghazi, which was likely due to the inclusion of individuals at higher risk. Significant predictors included ocular inflammation, elevated left eye IOP, and family history of glaucoma.

The high prevalence observed in our cohort (44.5%) was substantially higher than population-based studies in the region (e.g., 0.97% in Bahrain, [13] 1.92% in Iran,[14] 1.3% in Egypt [15]). The higher prevalence in our study was likely due to the sampling method, a glaucoma screening program that recruits a pre-diagnosed or high-risk population via local media.

Our findings on a positive family history doubling the risk (OR= 2.08, p= 0.016) aligned with other studies, [11, 16,17] and established literature that underscores the genetic component of the disease. [18]

The strongest predictor identified was a history of ocular inflammation, which increased the odds of glaucoma diagnosis by more than fivefold (OR = 5.2). This supports prior research on uveitic glaucoma [19] and emphasizes the need for early IOP monitoring in all patients with a history of inflammatory conditions in Libya, as inflammation can lead to secondary glaucoma due to trabecular meshwork damage or obstruction. [19]

The finding that left eye IOP was a significant predictor (p=0.003) while the right eye IOP was not, suggests a possible inter-eye asymmetry. While increased IOP was a major, well-established risk factor, [11, 15] the lateralized finding in this cohort warrants further investigation. This asymmetry might be due to differences in measurement or subtle anatomical factors, but it remained a strong, localized indicator in the current study.

Age was a well-established risk factor for glaucoma, with prevalence increasing significantly in older adults. Needlan et al. [20] found that glaucoma became more common after age 60. Zhang et al., [21] in a meta-analysis, noted the highest glaucoma risk in those over 80. In this study, our categorical risk plots similarly indicated higher rates in the 61–80 and >80 age brackets, but regression analyses did not show age as a statistically significant predictor. This discrepancy could be due to a smaller sample of older participants or confounding variables.

Gender's association with glaucoma diagnosis was inconsistent. Males had higher odds of diagnosis (OR = 1.85, p = 0.02 in Model 2), but this was not uniform across models. Some studies report higher male prevalence,[13,14,21] while others find higher rated or incidence in females. [22,23] Several studies found minimal or no sex differences, [15, 24] implying possible population-specific genetic or hormonal influences.

Although prior studies had suggested a higher prevalence of glaucoma in non-White, especially Black and mixed-race, groups.[25,286] The geographic and demographic characteristics of our study— predominantly White populations- may explain why race was not a significant predictor in our analysis. The absence of a significant link between race and glaucoma could also result from the small proportion of Black participants (6.3%, or 23 individuals).

Myopia and eye trauma were not significantly linked to glaucoma risk in this study, unlike previous reports suggesting severe myopia and eye trauma increase such risk.[27,28] This difference may result from variability in myopia severity or trauma among subjects.

Descriptively, optic disc cupping correlated strongly with glaucoma severity ($p < 0.001$): confirmed cases had larger cupping than suspects, underscoring the diagnostic value of optic nerve head evaluation, as also shown by Quigley et al.[29] However, after adjustment in multinomial

 ISSN: Online 2790-1637, Print 2790-1629
National Library of Libya, Legal number: 154/2018

logistic regression, optic disc cupping was not an independent predictor, possibly due to collinearity with IOP or age, or smaller numbers within subcategories.

This study found no significant association between systemic conditions (diabetes, hypertension, migraine, smoking, or ischemic heart disease) and glaucoma risk ($p > 0.05$ for all). Although some research tied diabetes and hypertension to glaucoma, likely due to vascular dysregulation, the discrepancy here may result from differences in disease severity or control. Supporting these findings, Torabi et al. [30] found no significant link between diabetes mellitus and glaucoma. Zhau et al. [31] reported a slightly higher glaucoma incidence in diabetics but no connection with DM duration. Langman et al. [32] identified hypertensions as more common in glaucoma patients and suggested β-blockers may offer some protection. Age and cardiovascular disease could independently influence glaucomatous neuropathy (Hayreh SS), [33] and a higher frequency of ischemic heart disease occurs in glaucoma cases (Chen et al.). [34] Despite previous suggestions, this study also found no smoking-glaucoma link, consistent with other studies. [35,35]

5.CONCLUSION

The high prevalence of glaucoma among adults in Benghazi was strongly associated with ocular inflammation, increased left-eye IOP, and family history. Policymakers and health care providers should use these findings to adopt more focused and effective screening methods. Screening should concentrate on older adults, those with a family history of glaucoma, and especially those who have had ocular inflammation. Directing resources toward these high-risk groups will improve early detection, support timely treatment, and help reduce preventable blindness in Libya.

This study had several limitations: Most participants were White or Libyan, which restricts the generalizability of the findings. The cross-sectional nature of the research means causality cannot be established. There was a risk of selection bias, as individuals who are more health-conscious may have been more likely to participate. Inconsistencies in the examiner's evaluations of IOP and optic disc could decrease the accuracy of the results. The small number of participants in the minority subgroup reduced statistical power, and not distinguishing glaucoma type limits the analysis of risk factors

The results highlighted the importance of targeted glaucoma screening for individuals with a history of ocular inflammation or glaucoma in their family. Including such an approach in community health initiatives may improve early diagnosis rates, decrease incidences of blindness, and guide policy decisions to better control glaucoma in Libya.

REFERENCES

1.Foster PJ, Buhrmann R, Quigley HA, Johnson GJ, The definition and classification of glaucoma in prevalence surveys. Br J ophthalmol 2002;358:238-42.

3.Mehta M, Mehta S, Bajaj S. Clinical profile, subtypes and risk factors among glaucoma patients in a tertiary hospital in Central India. Int J Sci Stud. 2017;4(11):107–12.

4.Kyari F, Entekume G, Rabiu M, et al. A population-based survey of the prevalence and types of glaucoma in Nigeria: results from the Nigeria National Blindness and visual impairment survey. BMC Ophthalmol. 2015;15(1):1–15.

5.Pascolini D, Mariotti SP. Global estimates of visual impairment: 2010. Br J Ophthalmol. 2012;96(5):614-618.

Tham YC, Li X, Wong TY, Quigley HA, Aung T, Cheng CY. Global prevalence of glaucoma and projections of glaucoma burden through 2040: a systematic review and meta-analysis. Ophthalmology. 2014 Nov;121(11):2081-90.

6.McMonnies CW. Glaucoma history and risk factors. J Optom. 2017;10(2):71-78. doi:10.1016/j.optom.2016.02.003

7.Obajolowo TS, Yusuf IA, Adeoti SG, Owoeye JFA, Taiwo MA, Olatunji FO. The Value of Targeted Screening for Glaucoma: The University of Ilorin Teaching Hospital Experience. West Afr J Med. 2024;41(7):741-747.

 ISSN: Online 2790-1637, Print 2790-1629
National Library of Libya, Legal number: 154/2018

8.Weinreb RN, Aung T, Medeiros FA. The pathophysiology and treatment of glaucoma: a review. JAMA. 2014;311(18):1901-1911. doi:10.1001/jama.2014.3192 Morgan IG, Ohno-Matsui K, Saw SM. Myopia. Lancet. 2012;379(9827):1739-1748.

9.Jonas JB, Aung T, Bourne RR, Bron AM, Ritch R, Panda-Jonas S. Glaucoma. Lancet. 2017;390(10108):2183-2193.

10.Vistamehr S, Shelsta HN, Palmisano PC, Filardo G, Bashford K, Chaudhri K, et al. Glaucoma screening in a high-risk population. J Glaucoma. 2006;15:534–540.

11.Ahmad SS. Glaucoma suspects: A practical approach. Taiwan J Ophthalmol. 2018;8(2):74-81.

12.Husain KA, Alaali H, Alarayedh GG. Prevalence and Characteristics of Glaucoma Among Patients Presenting to Ophthalmology Clinics in a Tertiary Hospital in the Kingdom of Bahrain. Cureus. 2024;16(2):e54129.

13.Hashemi H, Mohammadi M, Zandvakil N, et al. Prevalence and risk factors of glaucoma in an adult population from Shahroud, Iran. J Curr Ophthalmol. 2019;31(4):366-372.

14.Abd El-Basit A, Ismail A, Farouk M, El Saman I. "Prevalence of glaucoma among ophthalmology clinic patients at Sohag University Hospital". Egyptian Journal of Clinical Ophthalmology, 2023; 6(2): 153-164

15.Gordon MO, Beiser JA, Brandt JD, et al. The Ocular Hypertension Treatment Study: baseline factors that predict the onset of primary open-angle glaucoma. Arch Ophthalmol. 2002;120(6):714-820.

16.Priyadharshini SN, Bhuvaneswari KN. Study on prevalence of glaucoma among adult patients attending ophthalmology department in a tertiary care hospital, Kanchipuram. J Clin Images Med Case Rep. 2024; 5(3): 2947.

17.Abu-Amero K, Kondkar AA, Chalam KV. An Updated Review on the Genetics of Primary Open Angle Glaucoma. International Journal of Molecular Sciences. 2015; 16(12):28886-28911. https://doi.org/10.3390/ijms161226135

18.Rojas-Carabali W, Mejía-Salgado G, Cifuentes-González C, et al. Prevalence and clinical characteristics of uveitic glaucoma: multicentric study in Bogotá, Colombia. Eye (Lond). 2024;38(4):714-722. doi:10.1038/s41433-023-02757-9

19.Priyadharshini SN, Bhuvaneswari KN. Study on prevalence of glaucoma among adult patients attending ophthalmology department in a tertiary care hospital, Kanchipuram. J Clin Images Med Case Rep. 2024; 5(3): 2947

20.Zhang N, Wang J, Chen B, Li Y, Jiang B. Prevalence of Primary Angle Closure Glaucoma in the Last 20 Years: A Meta-Analysis and Systematic Review. Front Med (Lausanne). 2021;7:624179.

21.Kreft D, Doblhammer G, Guthoff RF, Frech S. Prevalence, incidence, and risk factors of primary open-angle glaucoma - a cohort study based on longitudinal data from a German public health insurance. BMC Public Health. 2019 Jul 1;19(1):851.

22.Mitchell P, Smith W, Chey T, Healey PR. Open-angle glaucoma and diabetes: the Blue Mountains eye study, Australia. Ophthalmology. 1997;104(4):712-718.

23.Tielsch JM, Katz J, Quigley HA, Javitt JC, Sommer A. Diabetes, intraocular pressure, and primary open-angle glaucoma in the Baltimore Eye Survey. Ophthalmology. 1995;102(1):48-53.

24.Protásio PSPGV, Almeida MDC, Maestri MK, et al. Exploring Associations between Race/Ethnicity and Glaucoma Prevalence in a Multicenter Brazilian Study: The ELSA-Brasil. Ethn Dis. 2025;35(1):27-34.

25.Yao M, Kitayama K, Yu F, Tseng VL, Coleman AL. Association Between Myopia and Primary Open-Angle Glaucoma by Race and Ethnicity in Older Adults in the California Medicare Population. JAMA Ophthalmol. 2023;141(6):525-532.

26.Marcus MW, de Vries MM, Junoy Montolio FG, Jansonius NM. Myopia as a risk factor for open-angle glaucoma: a systematic review and meta-analysis. Ophthalmology. 2011;118(10):1989-1994.e2.

27.Girkin CA, McGwin G Jr, Long C, Morris R, Kuhn F. Glaucoma after ocular contusion: a cohort

study of the United States Eye Injury Registry. J Glaucoma. 2005;14(6):470-473. doi:10.1097/01.ijg.0000185437.92803.d7

28.Quigley HA, Katz J, Derick RJ, Gilbert D, Sommer A. An evaluation of optic disc and nerve fiber layer examinations in monitoring progression of early glaucoma damage. Ophthalmology. 1992;99(1):19-28. doi:10.1016/s0161-6420(92)32018-4

29.Torabi R, Harris A, Siesky B, et al. Prevalence Rates and Risk Factors for Primary Open Angle Glaucoma in the Middle East. J Ophthalmic Vis Res. 2021;16(4):644-656.

31.Zhao D, Cho J, Kim MH, Friedman DS, Guallar E. Diabetes, fasting glucose, and the risk of glaucoma: a meta-analysis. Ophthalmology. 2015;122(1):72-78.

32.Langman MJ, Lancashire RJ, Cheng KK, Stewart PM. Systemic hypertension and glaucoma: mechanisms in common and co-occurrence. Br J Ophthalmol. 2005;89(8):960-963.

33.Hayreh SS. The role of age and cardiovascular disease in glaucomatous optic neuropathy. Surv Ophthalmol. 1999;43 Suppl 1:S27-S42

34.Chen YY, Hu HY, Chu D, Chen HH, Chang CK, Chou P. Patients with Primary Open-Angle Glaucoma May Develop Ischemic Heart Disease More Often than Those without Glaucoma: An 11-Year Population-Based Cohort Study. PLoS One. 2016;11(9):e0163210.

35.Doshi V, Ying-Lai M, Azen SP, Varma R; Los Angeles Latino Eye Study Group. Sociodemographic, family history, and lifestyle risk factors for open-angle glaucoma and ocular hypertension. The Los Angeles Latino Eye Study. Ophthalmology. 2008;115(4):639-647.e2.

36.Ramdas WD, Wolfs RC, Hofman A, de Jong PT, Vingerling JR, Jansonius NM. Lifestyle and risk of developing open-angle glaucoma: the Rotterdam study. Arch Ophthalmol. 2011;129(6):767-772.

 ISSN: Online 2790-1637, Print 2790-1629
National Library of Libya, Legal number: 154/2018